

Ion Effects on the Hyaluronan Secondary Structure in Computer Simulations and Experiments

Bc. Václav Buš

Master's thesis
2018



Tomas Bata University in Zlín
Faculty of Technology

Univerzita Tomáše Bati ve Zlíně

Fakulta technologická

Ústav fyziky a mater. inženýrství

akademický rok: 2017/2018

ZADÁNÍ DIPLOMOVÉ PRÁCE

(PROJEKTU, UMĚLECKÉHO DÍLA, UMĚLECKÉHO VÝKONU)

Jméno a příjmení: **Bc. Václav Buš**

Osobní číslo: **T16277**

Studijní program: **N2808 Chemie a technologie materiálů**

Studijní obor: **Materiálové inženýrství**

Forma studia: **prezenční**

Téma práce: **Vliv iontů na sekundární strukturu hyaluronanu v počítačových simulacích a experimentech**

Zásady pro vypracování:

1. **Prostudujte dostupnou literaturu a informační zdroje vztahující se k zadanému tématu.**
2. **Vypracujte literární rešerši na zadané téma.**
3. **Popište vliv iontů na sekundární strukturu hyaluronanu na základě simulací v programu NAMD a na základě experimentů.**

Rozsah diplomové práce:

Rozsah příloh:

Forma zpracování diplomové práce: **tištěná**

Seznam odborné literatury:

1. Mendichi R., Šoltés L., Schieroni A. G., Evaluation of Radius of Gyration and Intrinsic Viscosity Molar Mass Dependence and Stiffness of Hyaluronan. *Biomacromolecules* 4, 1805–1810 (2003).
2. Gribbon P., Heng B. C., Hardingham T. E., The analysis of intermolecular interactions in concentrated hyaluronan solutions suggest no evidence for chain-chain association. *Biochem. J.* 350, 329–335 (2000).
3. Gřundělová L., Mráček A. et al., The Influence of quarternary salt on hyaluronan conformation and particle size in solution. *Carbohydrate Polymers* 98, 1039–1044 (2013).
4. Iwahara J., Esadze A., Zandarashvili L., Review: Physicochemical Properties of Ion Pairs of Biological Macromolecules. *Biomolecules* 5, 2435–2463 (2015).

Vedoucí diplomové práce:

RNDr. Eva Kutálková, Ph.D.

Ústav fyziky a mater. inženýrství

Datum zadání diplomové práce:

2. února 2018

Termín odevzdání diplomové práce:

18. května 2018

Ve Zlíně dne 12. února 2018



doc. Ing. František Buňka, Ph.D.
děkan



doc. Mgr. Aleš Mráček, Ph.D.
ředitel ústavu

Příjmení a jméno: Buš Václav

Obor: Materiálové inženýrství.

PROHLÁŠENÍ

Prohlašuji, že

- beru na vědomí, že odevzdáním diplomové/bakalářské práce souhlasím se zveřejněním své práce podle zákona č. 111/1998 Sb. o vysokých školách a o změně a doplnění dalších zákonů (zákon o vysokých školách), ve znění pozdějších právních předpisů, bez ohledu na výsledek obhajoby ¹⁾;
- beru na vědomí, že diplomová/bakalářská práce bude uložena v elektronické podobě v univerzitním informačním systému dostupná k nahlédnutí, že jeden výtisk diplomové/bakalářské práce bude uložen na příslušném ústavu Fakulty technologické UTB ve Zlíně a jeden výtisk bude uložen u vedoucího práce;
- byl/a jsem seznámen/a s tím, že na moji diplomovou/bakalářskou práci se plně vztahuje zákon č. 121/2000 Sb. o právu autorském, o právech souvisejících s právem autorským a o změně některých zákonů (autorský zákon) ve znění pozdějších právních předpisů, zejm. § 35 odst. 3 ²⁾;
- beru na vědomí, že podle § 60 ³⁾ odst. 1 autorského zákona má UTB ve Zlíně právo na uzavření licenční smlouvy o užití školního díla v rozsahu § 12 odst. 4 autorského zákona;
- beru na vědomí, že podle § 60 ³⁾ odst. 2 a 3 mohu užit své dílo – diplomovou/bakalářskou práci nebo poskytnout licenci k jejímu využití jen s předchozím písemným souhlasem Univerzity Tomáše Bati ve Zlíně, která je oprávněna v takovém případě ode mne požadovat přiměřený příspěvek na úhradu nákladů, které byly Univerzitou Tomáše Bati ve Zlíně na vytvoření díla vynaloženy (až do jejich skutečné výše);
- beru na vědomí, že pokud bylo k vypracování diplomové/bakalářské práce využito softwaru poskytnutého Univerzitou Tomáše Bati ve Zlíně nebo jinými subjekty pouze ke studijním a výzkumným účelům (tedy pouze k nekomerčnímu využití), nelze výsledky diplomové/bakalářské práce využít ke komerčním účelům;
- beru na vědomí, že pokud je výstupem diplomové/bakalářské práce jakýkoliv softwarový produkt, považují se za součást práce rovněž i zdrojové kódy, popř. soubory, ze kterých se projekt skládá. Neodevzdání této součásti může být důvodem k neobhájení práce.

Ve Zlíně 14.5.2018

Tadeáš Buš

¹⁾ zákon č. 111/1998 Sb. o vysokých školách a o změně a doplnění dalších zákonů (zákon o vysokých školách), ve znění pozdějších právních předpisů, § 47 Zveřejňování závěrečných prací:

(1) Vysoká škola nevdělečně zveřejňuje disertační, diplomové, bakalářské a rigorózní práce, u kterých proběhla obhajoba, včetně posudků oponentů a výsledku obhajoby prostřednictvím databáze kvalifikačních prací, kterou spravuje. Způsob zveřejnění stanoví vnitřní předpisy vysoké školy.

(2) Disertační, diplomové, bakalářské a rigorózní práce odevzdané uchazečem k obhajobě musí být též nejméně pět pracovních dnů před konáním obhajoby zveřejněny k nahlášení veřejnosti v místě určeném vnitřním předpisem vysoké školy nebo není-li tak určeno, v místě pracoviště vysoké školy, kde se má konat obhajoba práce. Každý si může ze zveřejněné práce pořizovat na své náklady výpisy, opisy nebo rozmnoženiny.

(3) Platí, že odevzdáním práce autor souhlasí se zveřejněním své práce podle tohoto zákona, bez ohledu na výsledek obhajoby.

²⁾ zákon č. 121/2000 Sb. o právu autorském, o právech souvisejících s právem autorským a o změně některých zákonů (autorský zákon) ve znění pozdějších právních předpisů, § 35 odst. 3:

(3) Do práva autorského také nezasahuje škola nebo školské či vzdělávací zařízení, užije-li nikoli za účelem přímého nebo nepřímého hospodářského nebo obchodního prospěchu k výuce nebo k vlastní potřebě dílo vytvořené žákem nebo studentem ke splnění školních nebo studijních povinností vyplývajících z jeho právního vztahu ke škole nebo školskému či vzdělávacímu zařízení (školní dílo).

³⁾ zákon č. 121/2000 Sb. o právu autorském, o právech souvisejících s právem autorským a o změně některých zákonů (autorský zákon) ve znění pozdějších právních předpisů, § 60 Školní dílo:

(1) Škola nebo školské či vzdělávací zařízení mají za obvyklých podmínek právo na uzavření licenční smlouvy o užití školního díla (§ 35 odst. 3). Odpírá-li autor takového díla udělit svolení bez vážného důvodu, mohou se tyto osoby domáhat nahrazení chybějícího projevu jeho vůle u soudu. Ustanovení § 35 odst. 3 zůstává nedotčeno.

(2) Není-li sjednáno jinak, může autor školního díla své dílo užít či poskytnout jinému licenci, není-li to v rozporu s oprávněnými zájmy školy nebo školského či vzdělávacího zařízení.

(3) Škola nebo školské či vzdělávací zařízení jsou oprávněny požadovat, aby jim autor školního díla z výdělku jím dosaženého v souvislosti s užitím díla či poskytnutím licence podle odstavce 2 přiměřeně přispěl na úhradu nákladů, které na vytvoření díla vynaložily, a to podle okolností až do jejich skutečné výše; přitom se přihlédne k výši výdělku dosaženého školou nebo školským či vzdělávacím zařízením z užití školního díla podle odstavce 1.

ABSTRAKT

Molekulová dynamika simuluje chování systémů na základě řešení pohybových rovnic jednotlivých atomů, přičemž vychází z párových vazebných a nevazebných interakcí mezi atomy. Díky nižší časové i finanční náročnosti oproti reálným experimentům jsou metody molekulové dynamiky stále častěji využívány ke studiu struktury a vlastností makromolekul.

Cílem práce je popsat vliv různých iontů na strukturu hyaluronanu na základě simulací v programu NAMD, navrhnout charakteristiky náhodného klubka, které by možné srovnat s experimenty, a tyto charakteristiky následně naměřit pomocí dostupných experimentálních metod.

Klíčová slova: molekulová dynamika, polysacharid, gyrační poloměr, hydrodynamický poloměr

ABSTRACT

Molecular dynamics is a technique for computer simulations of complex systems, based on the bonded and non-bonded interactions between all pairs of atoms. These methods are more and more often used to investigate the structure and properties of molecules, because computer modelling is faster and less expensive than real experiments.

This thesis is focused on hyaluronan-ions effects using the molecular dynamics software NAMD. Appropriate characteristics of hyaluronan random coils ought to be suggested, calculated from simulations and measured using available experimental methods.

Keywords: molecular dynamics, polysaccharide, radius of gyration, hydrodynamic radius

ACKNOWLEDGEMENTS

I would like to thank my supervisor RNDr. Eva Kutálková, Ph.D. for valuable advice, provided background and time spent on my work. Furthermore, I would like to thank the National Grid Infrastructure Metacentrum for allowing me an access to computing and storage facilities within the Large Infrastructure Program LM2015042 E-Infrastructure CESNET and LM2015085 CERIT Scientific Cloud. I would like to thank Ing. Lenka Musilová, Ph.D. for valuable advice and time dedicated to experimental measurements and RNDr. Marek Ingr, Ph.D, for lending me a program for the creation of macromolecular coils.

I declare that the submitted version of the master's thesis and the electronic version uploaded to IS / STAG are identical.

CONTENTS

INTRODUCTION	9
I THEORY	10
1 HYALURONIC ACID	11
1.1 BIOLOGICAL FUNCTION AND APPLICATIONS	11
1.2 PHYSICAL AND CHEMICAL PROPERTIES	12
2 METHODS	14
2.1 MOLECULAR DYNAMICS	14
2.1.1 FORCE FIELDS	14
2.1.2 RADIUS OF GYRATION	17
2.1.3 PREVIOUS RADIUS OF GYRATION STUDIES	18
2.2 DYNAMIC LIGHT SCATTERING	23
2.2.1 HYDRODYNAMIC RADIUS	24
2.2.2 PREVIOUS HYDRODYNAMIC RADIUS STUDIES	25
II. ANALYSIS	27
3 PREPARATION AND MEASURING PROCESSING	28
3.1 RADIUS OF GYRATION	28
3.1.1 SYSTEM PREPARATION FOR MEASURING	28
3.1.2 MEASUREMENT OF THE RADIUS OF GYRATION	29
3.1.3 MD SIMULATIONS EQUILIBRIUM.....	30
3.2 HYDRODYNAMIC RADIUS	31
3.2.1 SAMPLE PREPARATION	31
3.2.2 MEASUREMENT ON ZETASIZER NANO ZS.....	32
4 RESULTS AND DISCUSSIONS	33
4.1 RADIUS OF GYRATION	33
4.1.1 INFLUENCE OF INTERACTION BETWEEN TWO HA CHAINS	33
4.1.2 RESULTS.....	34
4.2 HYDRODYNAMIC RADIUS	38
4.2.1 INFLUENCE OF DISTRIBUTIONS.....	38
4.2.2 RESULTS.....	42
CONCLUSION	45
BIBLIOGRAPHY	47
LIST OF ABBREVIATIONS	51
LIST OF FIGURES	52
LIST OF TABLES	54
APPENDICES	55

INTRODUCTION

Hyaluronic acid is a natural, non-linear, high molecular weight polysaccharide that has a high potential for the future in science and for humanity itself. Its origins date back to the 1930s, when hyaluronic acid was not yet sufficiently researched material. From the beginning, hyaluronic acid only served as a substitute for egg white in bakery products. Today, thanks to science and evolving technologies and knowledge of preparation or new modifications, it has begun to be used in various areas of human life, such as in tissue engineering, wound healing and burns research in cosmetics. Great hopes are being put into the research of anti-cancer treatment using hyaluronic acid or 3D printing.

Due to the development of various computing technologies, it is possible to study hyaluronan under experimentally poorly accessible conditions such as extreme temperatures and pressures and to learn more about the interaction of hyaluronan with other substances. Subsequently it is possible to study properties of the macromolecule such as a particle size. To study hyaluronan, a method of molecular dynamics can be used, which simulates the time evolution of physico-chemical properties of a given system with a large number of degrees of freedom based on the numerical solution of the equations of motion of individual atoms. Molecular dynamics methods are less expensive than real experiments, so they can be an interesting supplement of experiments.

This master's thesis describes the influence of various ions on the resulting structure of the HA macromolecule based on molecular dynamics simulations in NAMD software and experiment, using the method of dynamic light scattering. The main goal of this thesis is to find and perform a possible comparison between these two methods. There is a certain advantage that the NAMD software package is freely available for students and academics and there exists the MetaCentrum, which is also freely available for academics and students.

I. THEORY

1 HYALURONIC ACID

Hyaluronic acid (HA) is a high molecular weight biopolysaccharide (kDa – MDa) uncovered by Karl Meyer and his assistant John Palmer in the vitreous of bovine eyes in the 1930's. HA is a naturally occurring biopolymer in bacteria and higher animals including humans, which has important biological functions [1].

1.1 Biological functions and applications

HA primarily appears in extracellular and pericellular matrix. It can be found in most connective tissues and is specifically concentrated in synovial fluid, the vitreous fluid of the eye, umbilical cords and chicken combs. Almost half of the human body's HA occurs in skin with most of the HA situated in the intracellular space, where it may reach 2.5 g/l [2].

One the most important biological functions of the HA is elastic stability of liquid connective tissues such as articular synovial and eye glasses. Furthermore, HA controls tissue hydration and water transport, supramolecular assembly of proteoglycans in the extracellular matrix, and numerous role-mediated receptors in cell cleavage, mitosis, migration, tumour development and metastasis and inflammation.

The other important role in our body is to bind water and lubricate moving parts of the body, such as joints and muscles. Due to its consistency and tissue-friendliness it can be used in skin care products as an excellent moisturizer.

HA is one of the most hydrophilic molecules in the nature and so it is a natural moisturizing substance. HA with a unique viscoelastic nature, together with its biocompatibility and non-immunogenicity, is important for use in many clinical applications, including articular arthritis replacement [1].

Another important function of HA is a protection between the underlying tissues and the hostile environment. HA plays a role of a scavenger of free radical generated by the ultraviolet rays from sunlight [2].

The future of hyaluronic acid is probably mostly associated with tissue engineering, 3D technology and nano spinning. The use of a dual-cross-linking hyaluronic acid system as a printable hydrogel ink, which encompasses both shear-thinning and self-healing behaviours through guest-guest bonding as well as covalent cross-linking for stabilization using photopolymerization. The spinning process has emerged from

technologies that have long been known in the textile industry - from wet spinning and fiber drawing. Based on these known processes, a new technological process has been developed. The hyaluronic acid polymer initially enters the wet spinning process, during which it firstly dissolves in a water bath and then precipitates in the anti-solvent to form a fiber [3, 4].

1.2 Physical and chemical properties

It has been reported that HA in aqueous solution passes from the Newtonian to non-Newtonian characteristics with increasing molecular weight, concentration, or shear rate. In addition, with higher molecular weight and concentration of HA, the viscoelasticity of the solutions increases. The viscoelasticity of HA in aqueous solution is pH and ionic strength dependent. HA pKa values are about 3.0 [5], and therefore the change in pH affect the ionization of HA chains, and the subsequent change in ionization changes the intermolecular interaction between HA molecules that alters the rheological properties of the compound.

From a chemical point of view, it is a polysaccharide with repeating units of D-glucuronic acid and N-acetyl-D-glucosamine. The chemical structure was firstly determined by Weissman and Myer in 1954.

The primary structure of the polysaccharide contains an unbranched linear chain with monosaccharides linked together by alternating β -1.3 and β -1.4 glycosidic bonds –see Figure. 1a. Within the secondary structure of HA hydrophobic faces exist, formed by the axial hydrogen atoms of about eight CH groups on the alternating sides of the molecule. Such hydrophobic patches energetically support the formation of meshwork-like β -sheet tertiary structure as a result of molecular aggregation –see Figure 1b. The tertiary structure is stabilized by the intermolecular hydrogen bonding. The hydrophobic interaction and hydrogen bonding in combination with electrostatic repulsion allow large numbers of molecules to aggregate to the formation of molecular networks (matrices) of HA –see Figure 1c [5].

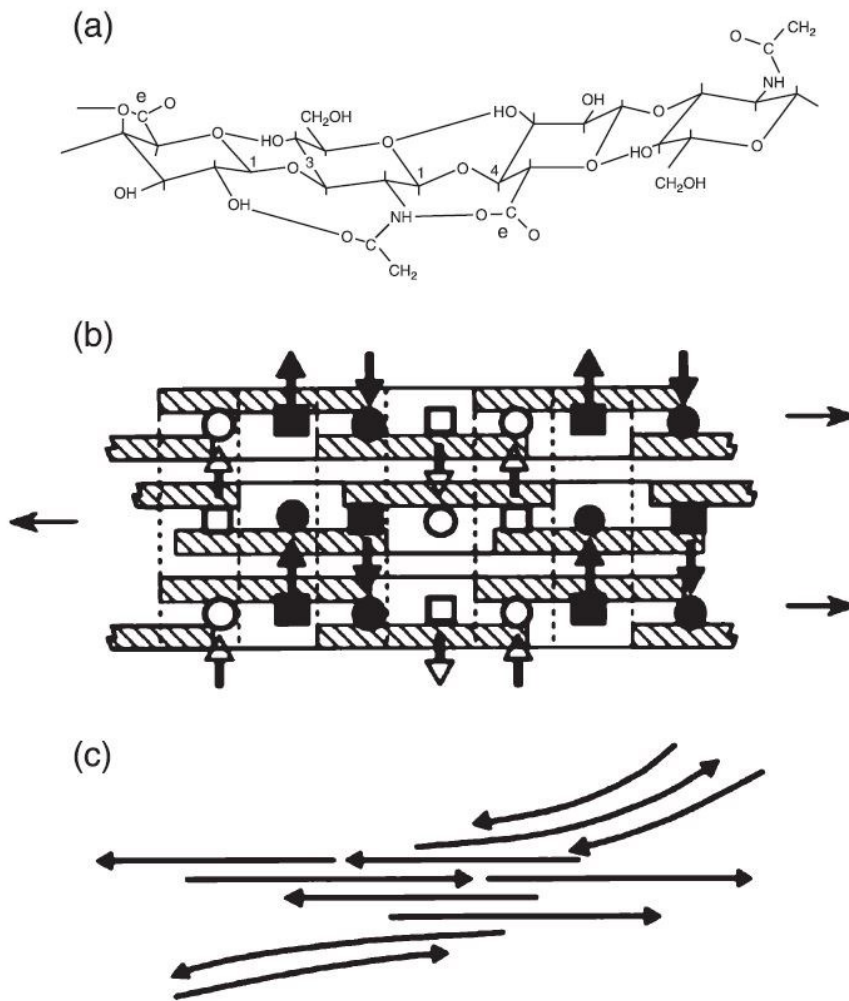


Figure 1 – The primary, secondary and tertiary structures of HA in solutions. (a) The primary structure of HA consists of repeating disaccharide units of D-glucuronic acid and N-acetyl-D-glucosamine with up to five hydrogen bonds existing between each two neighbouring disaccharides, while the secondary structures are formed as tape-like twofold helices by twisting each disaccharide unit through 180° compared with those ahead and behind it in the chain. (b) The β -sheet tertiary structure tertiary structure is energetically stabilized by interactions between hydrophobic patches (hatched) and intermolecular hydrogen bonding between the acetamido (\blacksquare and \square) and carboxylate groups (\bullet and \circ). (c) Schematic networks of HA molecules as a results of inter-molecular aggregation. [5]

2 METHODS

2.1 Molecular dynamics

Individual particles of macromolecules and their environment are in molecular dynamics (MD) modeled by solving the classical equations of motion (Newtonian equations of motion)

$$m_{\alpha} \ddot{\vec{r}}_{\alpha} = - \frac{\partial}{\partial \vec{r}_{\alpha}} U_{total} (\vec{r}_1, \vec{r}_2, \dots, \vec{r}_N), \alpha = 1, 2 \dots N, \quad 1.$$

where m_{α} is the mass of atom α , \vec{r}_{α} is its position and U_{total} is the total potential energy that depends on all atomic positions and, thereby, couples the motion of atoms.

The total potential energy, represented by the MD „force field”, the most necessary part of the simulation, must represent the interaction between atoms in a simple mathematical form that can be calculated quickly.

2.1.1 Force fields

MD is based on pair interactions between individual atoms. The potential energy function has following contributions:

$$U_{total} = U_{bond} + U_{angle} + U_{dihedral} + U_{vdW} + U_{Coulomb} + U_{imp} \quad 2.$$

The first three terms describe the stretching, bending, and torsional bonded interactions,

$$U_{bond} = \sum_{bonds\ i} k_i^{bond} (r_i - r_{0i})^2, \quad 3.$$

$$U_{angle} = \sum_{angles\ i} k_i^{angle} (\theta_i - \theta_{0i})^2, \quad 4.$$

$$U_{dihedral} = \sum_{dihedral\ i} k_i^{dih} [1 + \cos(n_i \varphi_i - \gamma_i)], \quad 5.$$

where bonds represent covalent bond in the system, angles are the angles between each pair of covalent bonds sharing a single atom at the vertex, and dihedrals describe atom pairs

separated by exactly three covalent bonds with the central bond subjected to the torsion angle φ .

The final three terms in equation 2 describe interactions between non-bonded atom pairs:

$$U_{imp} = \sum_{angles} K_{\psi} \cdot (\psi - \psi_0)^2, \quad 6.$$

$$U_{vdW} = \sum_i \sum_{j>1} 4\epsilon_{ij} \left[\left(\frac{\sigma_{ij}}{r_{ij}} \right)^{12} - \left(\frac{\sigma_{ij}}{r_{ij}} \right)^6 \right], \quad 7.$$

$$U_{Coulomb} = \sum_i \sum_{j>1} \frac{q_i q_j}{4\pi\epsilon_0 r_{ij}}, \quad 8.$$

vdWs correspond to the van der Waal's forces (approximated by a Lennard-Jones 6–12 potential), Coulombs represent electrostatic interactions and "Improper" monitor the planarity of planar structures [6, 7].

The basic principle of calculations is shown in Figure 2 [8].

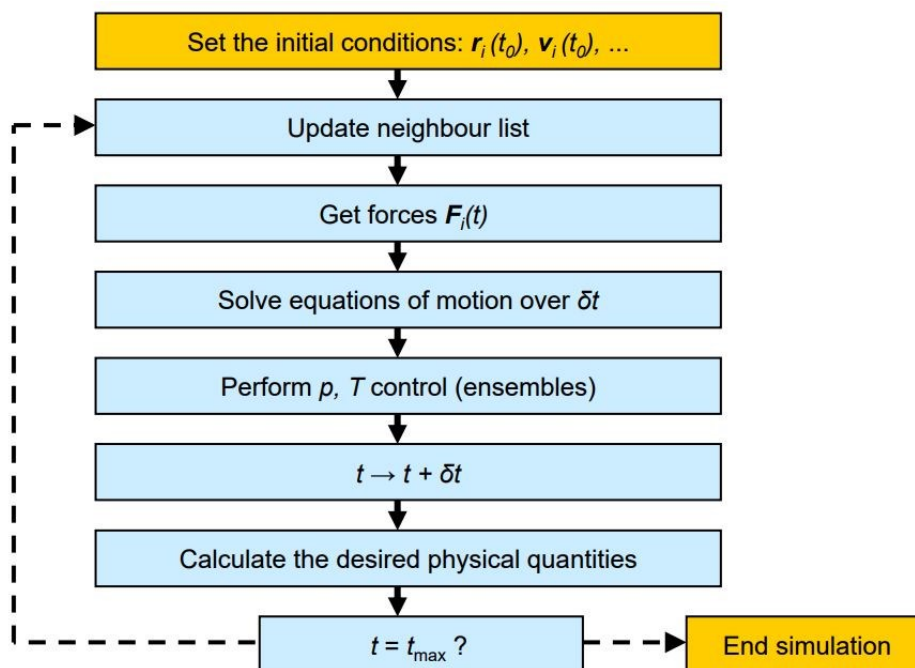


Figure 2 – Basic principle of calculation

All MD simulations were performed in NAMD 2.10 program package [9] using the CHARMM36 carbohydrate topology and force field parameters [10]. Long-range interactions (especially coulombic) were counted only within a certain “cutoff” distance, with the potential dropping linearly to zero from the distance "switchdist" - see Figure 3 [9].

Couples for which interactions were counted are within a distance marked "pairlistdist". The „timestep“ is limited by the vibration velocities of the lightest atoms and is usually 1 fs, exceptionally 2 fs. The coulombic potential is counted in the "cutoff" limit for each nth ("nonbondedFreq") time step. Except for this distance, coulombic interactions are calculated using the Particle Mesh Ewald method (PME), which, due to the reduction in computational difficulty, calculates the coulombic interactions only in certain places and therefore estimates the potential at other points. Every full step ("fullElectFrequency") the software calculates full electrostatics. With the "excluded scaled 1-4" value, all 1-3 pairs are excluded from the electrostatic calculation (i.e. if A is an atom bound to atom B and B is a carbon atom bound and atom C, which is attached to atom D, then the pair AD is excluded because the binding interactions between the atoms are much stronger than electrostatics). This interaction is replaced by “1-4scaling” [6, 11].

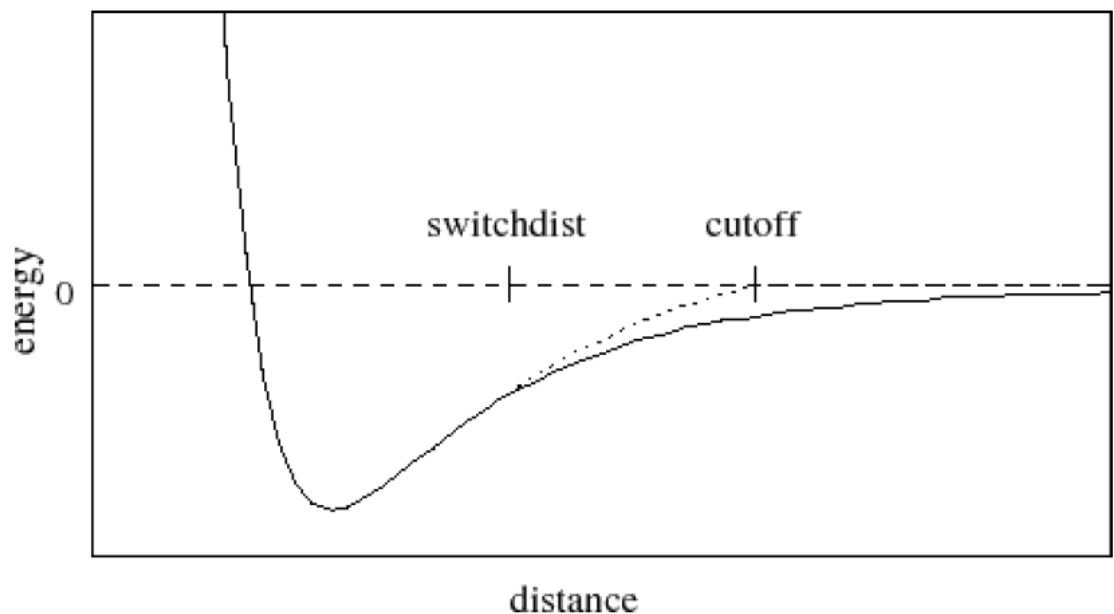


Figure 3 – Graph of VDW potential with and without cutoff function

2.1.2 Radius of gyration

Radius of gyration (R_g) is a parameter that describes the equilibrium conformation of a total system and is computed in two steps [12]. In the first step, the coordinates of the center of mass R_C are determined, ignoring the hydrogen atoms, from the following equation:

$$\sum m_i(r_i - R_C) = 0, \quad 9.$$

where m_i is the mass of the i -th atom and r_i is its position.

If atoms are taken as points in a 3D space, the square of the radius of gyration is acquired as

$$R_g^2 = \sum \frac{m_i(r_i - R_C)^2}{M}, \quad 10.$$

where M is the total mass of the atoms in a substance.

In the case of proteins, it is possible to assume equal masses for all non-hydrogen atoms so that

$$R_g^2 = \sum_{i=1}^N \frac{(r_i - R_C)^2}{N}, \quad 11.$$

where N is the number of atoms other than hydrogens in a substance.

The difference between the R_g values computed from Equations 10 and 11 is within several hundredths of angstrom. It is more important in terms of accuracy to consider atoms as coils with a radius R rather than as material points. Assuming that all atoms have the same radius (1.5 Å), we obtain a more exact equation:

$$R_g^2 = \sum_{i=1}^N \frac{(r_i - R_C)^2}{N} + \frac{3}{5}R^2. \quad 12.$$

In Equation 12, $\frac{3}{5}R^2$ is the square radius of gyration of a coil with the radius R and a uniform density:

$$\frac{\int_0^R r^2 4\pi r^2 dr}{\int_0^R 4\pi r^2 dr} = \frac{3}{5}R^2 \quad [12]. \quad 13.$$

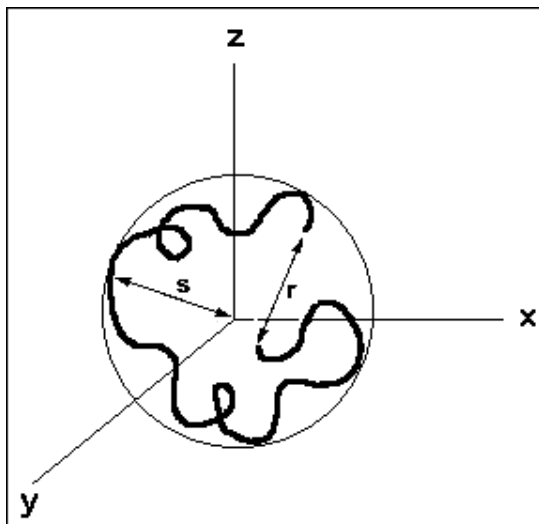


Figure 4 – Radius of gyration (s) [13]

2.1.3 Previous radius of gyration studies

2.1.3.1 Experimental studies

Sorci and Reed [14] studied the effect of addition of a certain type of salt (for example NaCl and CaCl₂) for different ionic strengths on the resulting radius of gyration of HA. (HA sodium salt (NaHy) was purchased from Sigma, separate gel permeation chromatography determinations gave $M_w = 1.8$ MDa.) The result is a plot of the radius of gyration dependence on the increasing ionic strength. Up to the value of $I = 2$ mM, the HA is gradually formed to a final value of about 2000 Å. Then, the HA structure is stabilized with salt. Since the value of $I = 5$ mM, there is a gradual linear decline in the radius of gyration. Monovalent salts exhibit compared to divalent higher value of the radius of gyration. The size of NaHy was 1760 Å and for HA calcium salt (CaHy) is 1550 Å (for $I = 100$ mM) –see Figure 5.

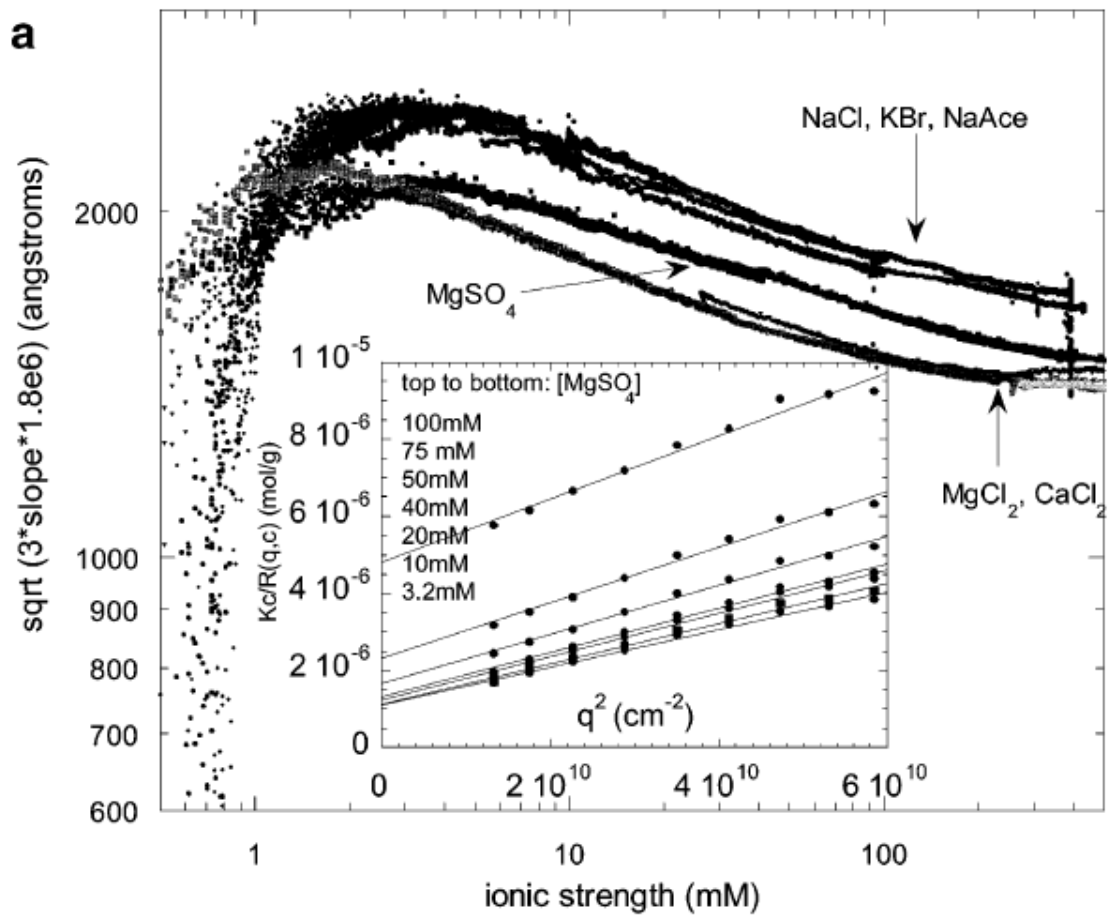


Figure 5 – Dependence of radius of gyration on ionic strength [14]

In the paper from Fouisacc et al [15] called "Influence of the Ionic Strength on the Dimensions of Sodium Hyaluronate" some of results are discussed about radius of gyration and persistence length for different molecular weights (0.13 – 1.86 MDa) of HA samples and three external salt contents with concentration (0.01; 0.06 and 0.3 M) using light scattering. The results are shown in the Figure 6.

M_w	L (Å)	C_s (N)	$(\rho^2)_z^{1/2}(\text{exptl})$ (Å)
1.86×10^6	46 500	0.3	1554
		0.06	1907
		0.01	2207
810 000	20 250	0.3	980
		0.06	1039
		0.01	1067
360 000	9 000	0.3	578
		0.06	592
		0.01	712
260 000	6 500	0.3	509
		0.06	
		0.01	608

Figure 6 – Radius of gyration results for different molecular weight M_w and concentration c [15]

In the article from Hayashi et al [16] „Chain-Stiffness and Excluded-Volume Effects in Solutions of Sodium Hyaluronate at High Ionic Strength“, twelve samples of NaHy were studied ranging in weight-average molecular weight from 3.8 to 350 kDa by static light scattering with 0.5 M aqueous NaCl at 25 °C –see Figure 7.

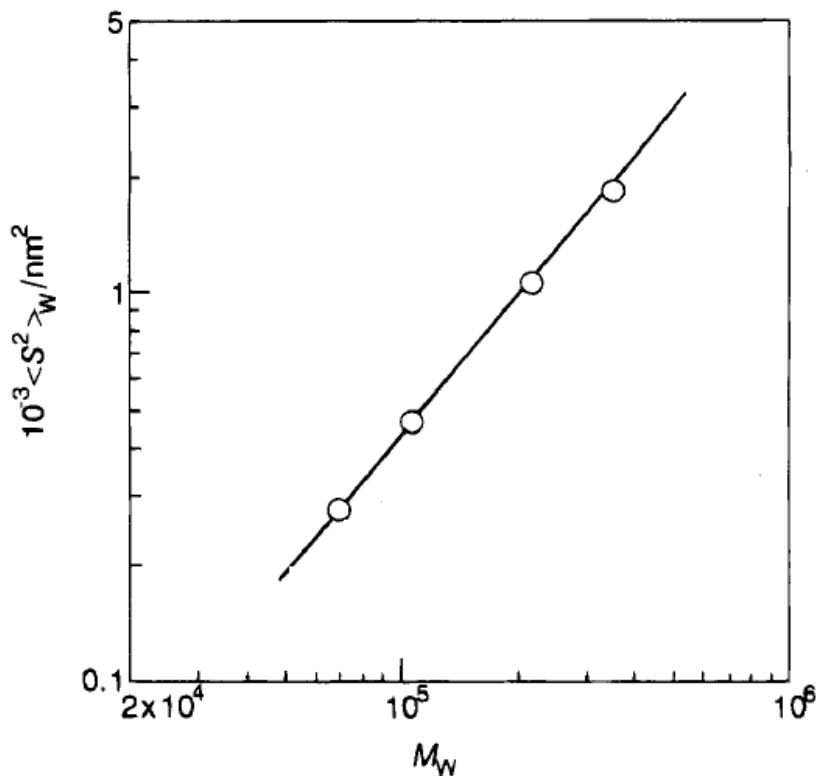


Figure 7 – Radius of gyration of NaHy for different M_w [16]

In the paper from Mendichi et al [17] „Evaluation of Radius of Gyration and Intrinsic Viscosity Molar Mass Dependence and Stiffness of Hyaluronan“, the radius of gyration (R_g) of nine HA samples with molecular mass ranging from 40 kDa to 5.5 MDa in 0.15 M NaCl at 37 °C was measured by on-line multiangle light scattering –see Table 1.

Table 1 – Results of radius of gyration for different M_w [17]

Sample	M_w (kDa)	R_g (Å)
HA_1	236	550
HA_2	580	890
HA_3	665	980

In the study „Chain Persistence Length and Structure in Hyaluronan Solutions: Ionic Strength Dependence for a Model Semirigid Polyelectrolyte“, Buhler and Boué [18] directly determined for the first time the structure and the chain conformation of hyaluronan, a model semirigid polyelectrolyte polysaccharide. In part of this study the radius of gyration of the HA of two different molecular weights in 0.1 M sodium solution by static light scattering was measured. The results of this measurement are shown in the Table 2.

Table 2 – Results of radius of gyration [18]

M_w [kDa]	R_g [Å]
85	270 ± 20
160	350 ± 40

2.1.3.2 MD studies

A study called “How Large is an α -Helix? Studies of the Radii of Gyration of Helical Peptides by Small-angle X-ray Scattering (SAXS) and Molecular Dynamics“[19] investigated the size of the radius of gyration of alanine-based helical peptides, measured by two methods, using SAXS and MD. Based on these measurements, gyration radii were compared with known sizes of ideal α -helixes. As a result, the radii of gyration of the peptides studied in this work are significantly smaller than the radii of gyration

of ideal α -helices with the same sequence length. The gyration radius values measured by the SAXS method were also less than with MD method.

In an article „Hyaluronan random coils in electrolyte solutions—a molecular dynamics study”, Ingr, Kutálková and Hrnčířik [20] have used the method of molecular dynamics to model random coils of hyaluronan. An oligosaccharide of 48 monosaccharide units was simulated until equilibrium (about 70 to 100 ns) and randomly selected pieces of the molecule from different simulation frames were combined to form a long polysaccharide chain of hyaluronan. The dihedral angles of the glycosidic connections of the pieces completed with statistics deduced from the simulation. Selected molecules were hyaluronan simulated in 1 M, 0.2 M and 0 M (polyelectrolyte only neutralized by counterions) and its non-charged analogue in which the glucuronic acid unit was substituted by glucose simulated in 1 M NaCl and MgCl₂ and in pure water.

Radius of gyration as a function of the number of monosaccharide units N for all the simulated systems are presented in the Figure 8.

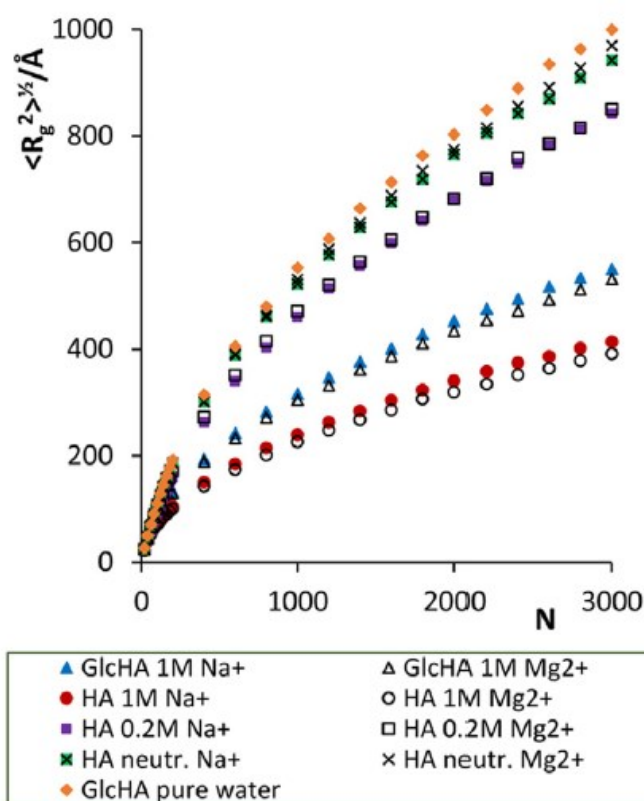


Figure 8 – Radius of gyration as a function of the number of monosaccharide units N for all the simulated systems [20]

Ivanov and Nematu [21] focused on comparing HA simulations in aqueous media and HA in aqueous media with different compounds. The main idea was to identify binding sites, determine the frequency of their occupation, and compare the affinity of molecules of various compounds and water.

Almond, DeAngelis, and Blundell [22] used MD simulations to study conformations and detect the valence and dihedral angles of HA compared with experimental data. The simulations were performed on tetrasaccharide and hexasaccharide of HA with an explicit aqueous solvent and addition of sodium ions to achieve neutrality.

2.2 Dynamic light scattering

Dynamic light scattering (DLS) [23] is the most adaptable and useful set of techniques for measuring in situ the sizes, and size distributions. There are many alternatives of DLS. DLS methods are not able to identify the chemical nature of a nanoparticle. They measure hydrodynamic quantities, usually the translational and/or rotational diffusion coefficients, which are then related to sizes and shapes via theoretical relations. DLS is a technique often referred to as photon correlation spectroscopy (PCS).

PCS is now the standard technique most commonly used in biophysical, colloidal and polymeric laboratories. It serves to routinely characterize the particles as well as to study the nature of the interactions of molecules and particles in liquid dispersions.

Figure 9 shows a diagram of a PCS device. Laser light is targeted at a sample and a light scattered at a given angle of scattering is collected by a square law detector – a photomultiplier, as it becomes more common, an avalanche photodiode. The output of the photomultiplier is then processed by the photon counting system and the output is sent to the autocorrelator. In modern PCS, fiber optic conductors are often applied to supply light to the sample and collect scattered light, which then transports into the detector. In fact, optical fibers are essential parts of this technique for heavily dispersed systems.

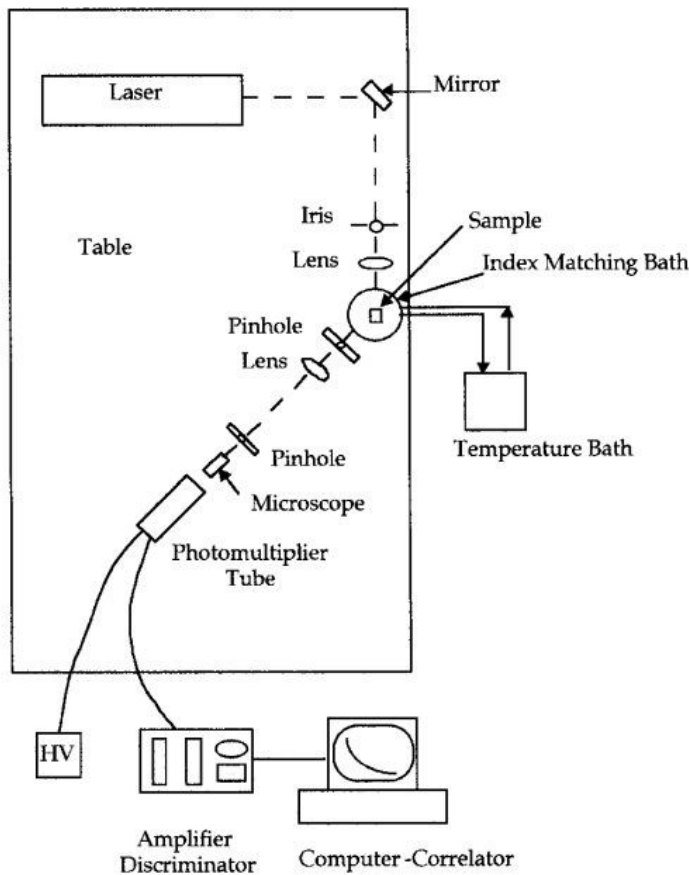


Figure 9 – Schematic diagram of a PCS apparatus [23]

2.2.1 Hydrodynamic radius

Particles suspended in a liquid solvent are subjected to a random Brownian motion. The light is scattered due to the particles in the suspension. Because the particles cause localized changes in the refractive index, intensity variations are made by the particles and evaluated using the second order normalized autocorrelation function [23, 24]

$$g_2(\tau) = \frac{G_2(\tau)}{\langle I \rangle^2}, \quad 14.$$

where $\langle I \rangle$ is the average intensity, τ is the correlation time, and $G_2(\tau)$ is the temporal correlation function.

The second order normalized correlation function is then connected to the first order correlation function $g_1(\tau)$, where $g_1(\tau)$ is expressed as

$$g_1(\tau) = e^{-q^2 D \tau}, \quad 15.$$

where q is the magnitude of the scattering vector and D is the translational diffusion coefficient.

The scattering vector q is calculated as

$$q = \frac{4\pi n}{\lambda_0} \sin\left(\frac{\theta}{2}\right), \quad 16.$$

where n is the refractive index of the solution, λ_0 is the wavelength of incident light in vacuum and θ is the scattering angle of light.

Using the Stokes-Einstein equation

$$D = \frac{kT}{6\pi\eta R_h}, \quad 17.$$

sizes of particles in the solution are finally determined (D is the diffusion coefficient, k is Boltzmann's constant, T is the temperature, η is the solvent viscosity, and R_h is the hydrodynamic radius of the particles in solution).

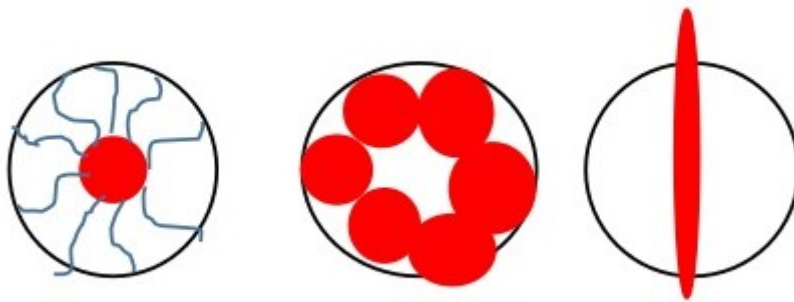


Figure 10 – Hydrodynamic radius (the size of a hypothetical hard sphere that diffuses in the same fashion as the particle being measured) [25]

2.2.2 Previous hydrodynamic radius studies

One study from Grundělová et al [26], which used DLS techniques to measure the change in HA size after the addition of a certain amount of salt, was a study called “The influence of quaternary salt on hyaluronan conformation and particle size in solution”. Measurements performed HA samples with two molecular weights ($M_w = 1.8$ MDa and $M_w = 0.35$ MDa). Benzalkonium chloride was used as the salt.

Another paper from Gribbon et al [27] “The analysis of intermolecular interactions in concentrated hyaluronan solutions suggest no evidence for chain–chain association” used DLS to study the influence of various salts (Ca^{2+} , Mn^{2+} , Mg^{2+} , Na^+ and K^+) on the HA hydrodynamic radius ($M_w = 830$ kDa) of the same concentration of salt ($c = 10$ mg/ml).

Analysis of DLS in the diluted solution showed a changes in the hydrodynamic radius HA, for example with CaCl₂ (36 nm) and with NaCl (43 nm).

Next article from Viletti et al [28] “Static and Dynamic Light Scattering of Polyelectrolyte/Surfactant Solutions: the Na-Hy / (C10TAB) System” discusses the interactions between the anionic polyelectrolyte NaHy and the cationic surfactant decyltrimethylammonium bromide (C10TAB). DLS experiments were carried out in the single homogenous phases (region I: [C10TAB] < 0.040 M and region III: [C10TAB] > 0.350 M) in “salt-free” and at different added salt concentrations (NaCl) – see Figure 11. The authors observed the decrease of the hydrodynamic radius with salt up to 150 mmol/l, whereas the hydrodynamic radius remained constant after a further increase in concentration.

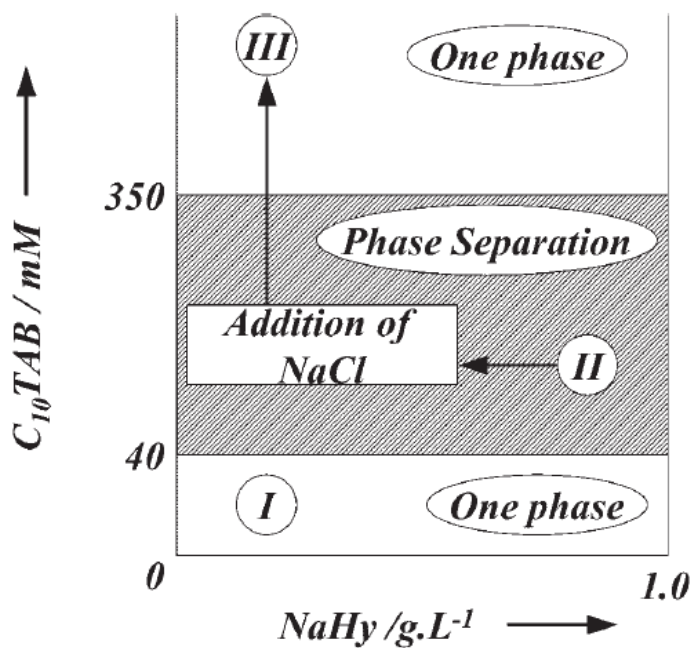


Figure 11 – Phase diagram of Na-Hy polyelectrolyte in C10TAB surfactant and NaCl salt. (I) homogeneous phase; (II) phase separation and (III) homogeneous phase after addition of salt or surfactant. [28]

II. ANALYSIS

3 PREPARATION AND MEASURING PROCESSING

The influence of ions and ionic strength on the size of HA was investigated through two basic characteristics: the radius of gyration and the hydrodynamic radius, which were then compared with each other.

3.1 Radius of gyration

3.1.1 System preparation

In the system under examination there were two antiparallel HA chains, each of which contained 24 pairs of monosaccharide units - see Figure 12. This system was solvated by a water box of (161.8 x 110.9 x 187.2) Å with an explicit model of water molecules TIP3P (in the systems with monovalent cations there were 310689 water molecules; with divalent cations 304722). Subsequently, the system was neutralized and salted with 6 different chlorides (NaCl, KCl, CsCl, MgCl₂, CaCl₂, ZnCl₂) to a final ionic strength of (0.2; 0.6 and 1) mol·l⁻¹ (in systems with monovalent salts there were 2061 cations and 2013 anions; for divalent salts 2037 cations and 4026 anions). Ionic strength 0.2 mol/l corresponds to 9.5 cations/dimer, 0.6 mol/l corresponds to 26 cations/dimer and 1 mol/l corresponds to 43 cations/dimer.

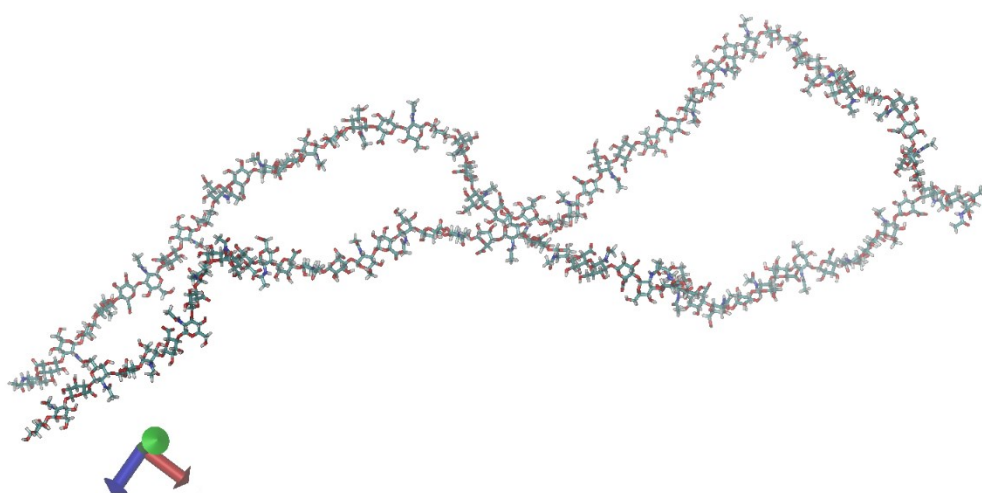


Figure 12 – Double-chain of HA

Both HA chains in the water were completely free during simulations. In the case where a part of the HA chain has got out of the water box, the water molecules positions were recalculated through periodic boundary conditions.

All simulations were performed using the NAMD version 2.10 [9] software package with CHARMM topologies and force field parameters. [10] Using the "automatic PSF builder" in NAMD, a so-called PSF file was created using a topological file that determines the pairing of individual atoms with other possible atoms. Timestep was set to 1 fs, cutoff 10 Å and switching 8 Å. The electrostatic effect was calculated using the PME, which is part of the NAMD program package. Non-binding interactions were calculated in every second step ("nonbondedFreq") and full electrostatics in every sixth step ("fullElectFrequency"). System energy was minimized for 180 fs, subsequent simulations were performed at a constant temperature of 310 K and at atmospheric pressure with periodic boundary conditions. The temperature was controlled by Langevin's dynamics. Coordinates of all atoms for subsequent display and data processing in VMDs were stored every 1800 fs. The simulation duration ranged from 75 to 85 ns. All parameters were set using the configuration file - see Appendix P I.

Inter-atomic distances and other geometric properties were evaluated using VMD 1.9.3. [29] MD calculations were very time consuming and hardware-intensive. There were therefore used the services of the National Grid Infrastructure MetaCentrum owning several supercomputers, which can be used for parallel computations on many processors. [11]

3.1.2 Measurement of the radius of gyration

To determine the radius of gyration of large HA random coils, a homemade program was applied to molecular-dynamics simulations results for the oligosaccharides of 48 monosaccharide units. Randomly selected pieces of the chain from different frames of the simulation were combined by a method of selection of the glycoside-bond dihedral angles in accord with their distribution in the simulated molecules, which allowed to create all-atom models of random coils of up to at least 5000 monosaccharide units.

Our method of construction of large macromolecular coils was similar to the method used by Furlan et al. [30] or Ivanov & Neamtu [21], but it was applied to much larger molecules and a specific statistical procedure to determine the dihedral angles of glycosidic connections of the pieces was used. Due to the purpose of monitoring the system in

equilibrium, the pieces for building of the random coils were taken from the interval of approximately 5 ns. For each such interval 5000 coils of a reference length of 2000 monosaccharides ($M_w = 379$ kDa) were generated and the mean square value of the radius of gyration and standard deviation of the mean value were calculated. The chosen length is adequate for the composition of a realistic random coil. This method was previously used by Ingr, Kutáľková & Hrnčířík. [24]

3.1.3 MD simulations equilibrium

MD simulation were calculated for individual systems with a duration of around 80 ns. The equilibrium for ion interaction with HA occurred as early as about 30 ns, when the dependence of the number of ions near the macromolecule on time fluctuated around the steady average - see Figure 13. For more relevant coil size results, only simulation sections with no interaction between the two chains (or the interaction as small as possible) were used. These sections were found after much longer simulation time.

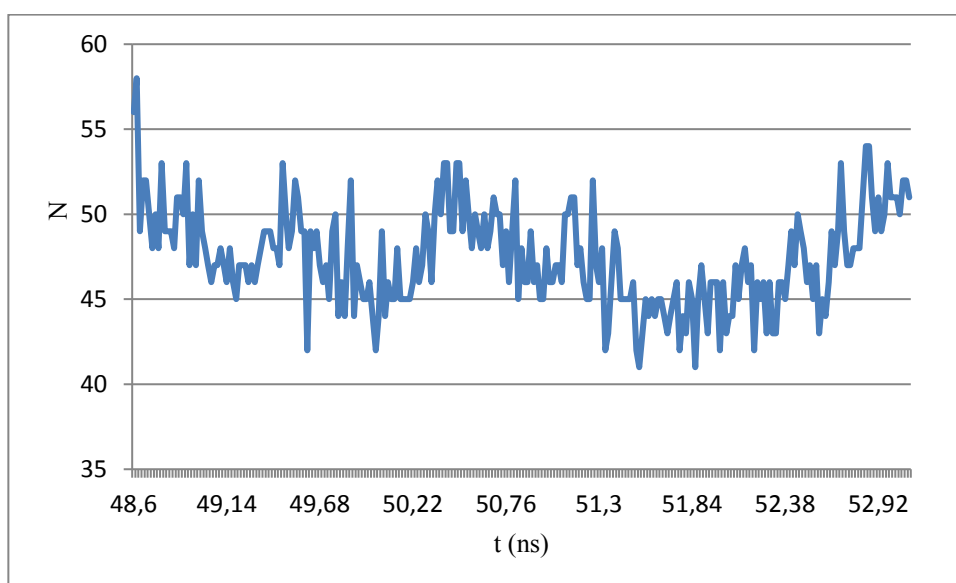


Figure 13 – Dependence of the mean number of Ca²⁺ ions N in the vicinity of HA on time

3.2 Hydrodynamic radius

3.2.1 Sample preparation

Three different molecular weights of HA (243, 370 and 600 kDa) were tested. For every molecular weight three different solutions of HA with three different salts (sodium chloride, calcium chloride and zinc chloride) at different concentrations (200, 600 and 1000 mmol/l) were prepared.

Firstly, a 100 ml salt solution was prepared with certain ionic strengths. For example, for NaCl with the ionic strength of 0.6 mol/l the relationship between the ionic strength and concentration is:

$$I_{NaCl} = \frac{1}{2} \sum_{i=1}^b c_i z_i^2 = \frac{1}{2} (2c) , \quad 18.$$

$$c_{NaCl} = I_{NaCl} = 0.6 \text{ mol/l} , \quad 19.$$

where c is concentration, z is charge and I is ionic strength.

Consequently, the NaCl weight is

$$m_{NaCl} = c_{NaCl} \cdot M_{NaCl} \cdot V_{NaCl} = 0.6 \frac{\text{mol}}{\text{l}} \cdot 58.44 \frac{\text{g}}{\text{mol}} \cdot 0.1 \text{ l} = 3.5064 \text{ g} , \quad 20.$$

where m is weight, M is molecular weight and V is volume.

Similarly, for CaCl₂ with 0.6 mol/l ionic strength.

$$I_{CaCl_2} = \frac{1}{2} \sum_{i=1}^b c_i z_i^2 = \frac{1}{2} (5c) , \quad 21.$$

$$c_{CaCl_2} = \frac{2}{5} I_{CaCl_2} = 0.24 \text{ mol/l} , \quad 22.$$

$$m_{CaCl_2} = c_{CaCl_2} \cdot M_{CaCl_2} \cdot V_{CaCl_2} = 0.24 \frac{\text{mol}}{\text{l}} \cdot 110.99 \frac{\text{g}}{\text{mol}} \cdot 0.1 \text{ l} = 2.6638 \text{ g} , \quad 23.$$

Subsequently, a 1% solution of HA was produced in a 25 ml flask by mixing 0.25 g of solid HA with 24.75 ml of salt solution prepared in the previous step. The flask with the 1%

HA solution was mixed in a mixer machine with water heated to the temperature of 50 °C for 24 hours (until complete HA dissolution).

3.2.2 Measurement on Zetasizer Nano ZS

The prepared solutions of HA were further diluted to the resulting 0.1% solution by adding of salt solution to be compatible with the measuring range of the Zetasizer Nano ZS [31]. The 1% solution of the lowest molecular weight HA (243 kDa) had to be finally diluted with an additional amount of salt solution to a final 0.05% solution.

The prepared HA solutions were then placed in special measurement cuvettes using a syringe with a sterile filter having a pore size of 0.2 µm. The cuvettes were then inserted into the measuring device.

The Zetasizer software requires certain information about the physical properties of the material and of the dispersant of the sample. It is therefore necessary to enter all these data into the measuring program, including the molecular weight of HA and concentration of the dispersant and the temperature at which the sample will be measured. Based on these data, the viscosity and refractive index of the measured sample are calculated, which is important for the final calculation of particle sizes. Longer measurement durations will increase the quality of data obtained and will generally give better results, as those runs that contain the poorest data, which have been rejected. Remaining good runs were used in the final measurement calculation. Because of the polydispersity, the number of measurements was 15 and the measurement duration was 60 seconds. Five measuring cycles were performed on each sample and the average particle distribution was then calculated.

4 RESULTS AND DISCUSSIONS

4.1 Radius of gyration

4.1.1 Influence of interaction between two HA chains

The simulated system consists of two antiparallel chains because we originally wanted to study hyaluronan-hyaluronan interactions and subsequently the influence of these interactions to their shape. Because the influence of salts on the HA radius of gyration is far more prominent, it was important to find the simulations sections without these interactions. The coil was then composed of only one chain. Table 3 shows electrostatic, vdW, and total nonbond values for individual systems. Maximum electrostatic interaction was at the system with calcium and zinc ions. These systems do not exactly match the model we need, there is no zero interference. On the contrary, the system with potassium and cesium ions show almost zero interaction between the two chains – see Figure 14. For systems that exhibit zero or smallest interaction, the influence of ions and their concentration on the final size of coil was studied.

Table 3 – Minimal HA-HA interaction energy values (kcal/mol) for individual systems from all simulation runs

	Ion	Elec	VdW	Nonbond
1 M	Na ⁺	0,91 ± 0,09	-0,13 ± 0,02	0,78 ± 0,08
	K ⁺	-0,0077 ± 0,0006	-0,00040 ± 0,00008	-0,0080 ± 0,0006
	Cs ⁺	4,05 ± 0,15	-1,17 ± 0,08	2,9 ± 0,1
	Ca ²⁺	56,1 ± 0,9	-21,1 ± 0,6	34,9 ± 0,8
	Zn ²⁺	89,9 ± 1,2	-45,8 ± 0,9	44,1 ± 0,9
	Mg ²⁺	7,5 ± 0,5	-1,27 ± 0,08	6,2 ± 0,4
600 mM	Na ⁺	24,1 ± 0,7	-12,6 ± 0,6	11,6 ± 0,6
	K ⁺	-0,72 ± 0,06	-2,6 ± 0,2	-3,3 ± 0,2
	Cs ⁺	1,76 ± 0,19	-0,46 ± 0,07	1,30 ± 0,09
	Ca ²⁺	9,8 ± 0,5	-10,7 ± 0,6	-0,93 ± 0,08
	Zn ²⁺	21,9 ± 0,6	-6,9 ± 0,4	15,0 ± 0,5
	Mg ²⁺	11,1 ± 0,4	-0,87 ± 0,07	10,2 ± 0,4
200 mM	Na ⁺	1,21 ± 0,09	-1,17 ± 0,13	0,036 ± 0,002
	K ⁺	0,078 ± 0,005	-0,026 ± 0,005	0,051 ± 0,005
	Cs ⁺	0,058 ± 0,004	-0,008 ± 0,002	0,049 ± 0,004
	Ca ²⁺	58,3 ± 0,8	-3,3 ± 0,1	55,0 ± 0,7
	Zn ²⁺	18,6 ± 0,6	-3,5 ± 0,2	15,1 ± 0,5
	Mg ²⁺	0,50 ± 0,06	-0,085 ± 0,008	0,42 ± 0,06

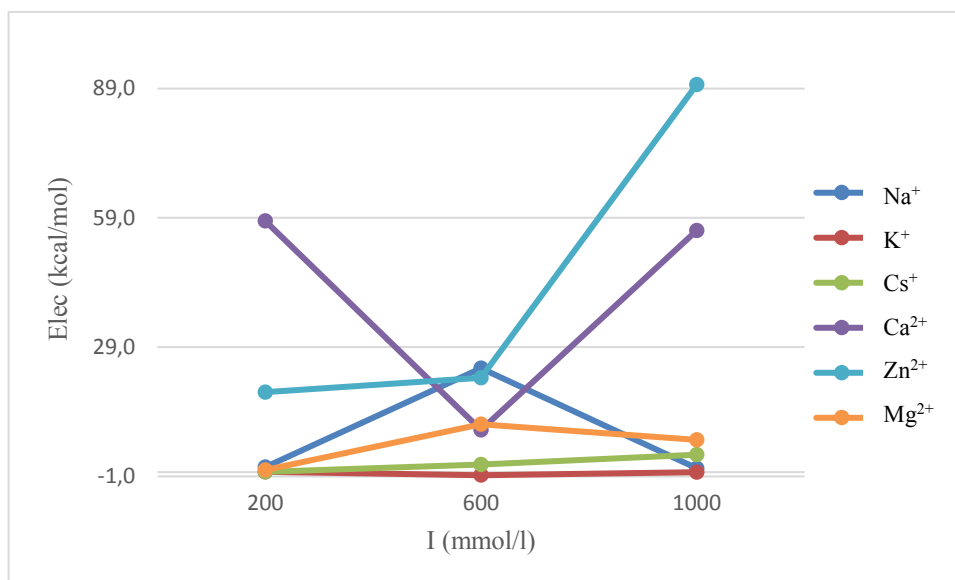


Figure 14 – Dependence of HA-HA electrostatic interactions on the ionic strength for individual systems (The error lines are hidden within individual points – small measurement errors)

4.1.2 Results

Figure 15 shows a trend where the radius of gyration of the coil is the largest for system with ionic strength of 600 mmol/l. At an ionic strength of 200 mmol/l, few ions are present in the vicinity of HA. It has caused a good dispersion of the ions in the small space of the coil and has not changed its size, so the radius of gyration is small. With the increase of ionic strength, the number of ions near the HA also increase –see Figure 16. After that, there was no good dispersion in the space of the coil and its expansion occurred, i.e. the increase in the radius of gyration was observed. The huge number of ions near the HA at the greatest ionic strength caused the overall stabilization of the coil. The resultant radius of gyration has returned to lower values.

The opposite trend only showed a system with calcium ions, which could be due to the high interaction between the two chains in this system and the large number of ions in the vicinity of HA at the lowest ionic strength.

The radius of gyration ranged from 300 Å to 865 Å for individual systems. Calculated for 2000 monosaccharide units (corresponds to a molecular weight of 370 kDa). The smallest size of the coil had a system with sodium ions (from 300 Å to 465 Å). In previous studies, the size of a coil in similar systems at 0.3 mol/l concentration was around 570 Å [15]. On the other hand, the system with zinc ions had a value of about 525 Å to 865 Å.

Stabilization of the coil occurred at the highest ionic strength. Higher size could also be caused by great interactions between chains in this system.

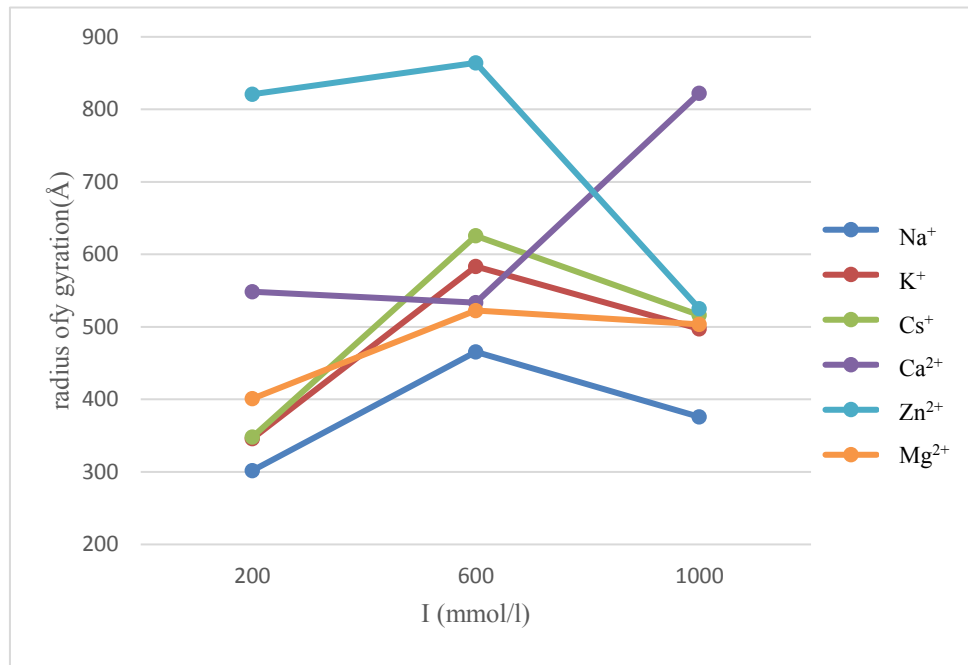


Figure 15 – Dependence of the radius of gyration on ionic strength for individual systems (The error lines are hidden within individual points – small measurement errors.)

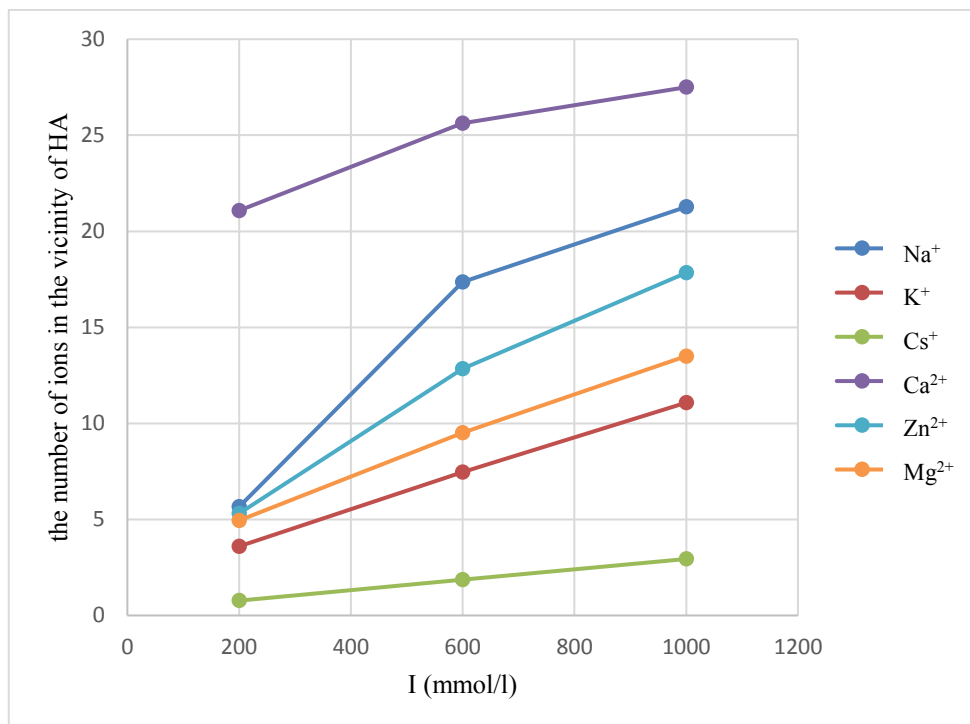


Figure 16 – Dependence of the number of ions in the vicinity of HA on ionic strength for individual systems (The error lines are hidden within individual points – small measurement errors.)

In the following three figures (Figure 17-19), dependence of the radius of gyration on the number of monosaccharide units for three different ionic strengths is shown, where the number of 3250 monosaccharide units corresponds to a molecular weight of approximately 600 kDa. Dependence showed a similar growing trend for all salts, with the exception of the system with zinc ions ($I = 200$ mmol/l), where the last two values deviated from the linear character. It could be caused by big interaction between two chains in this system. The radius of gyration was higher than 1000 \AA for the system with zinc ions with 3250 monosaccharide units. At the highest ionic strength, the gyration radius was reduced to about 670 \AA because of greater stabilization of the coil.

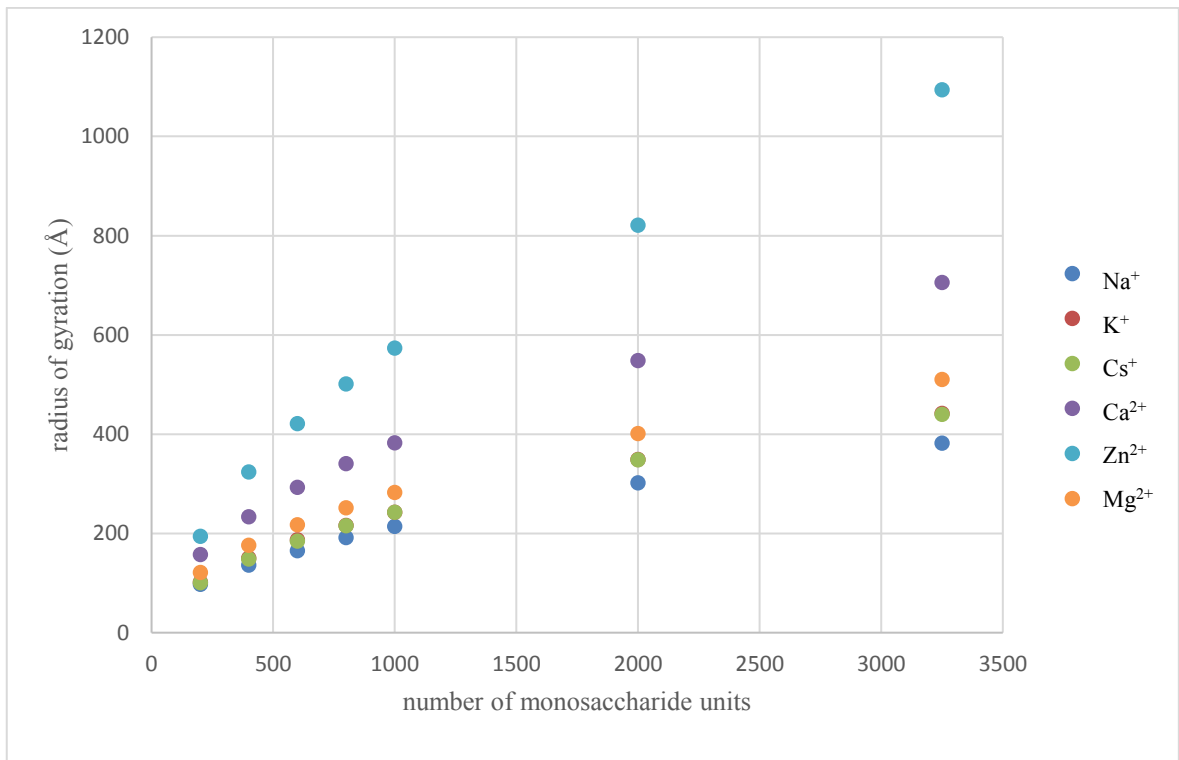


Figure 17 – Dependence of radius of gyration on the number of monosaccharide units ($I = 200$ mmol/l) (K^+ values are covered by Cs^+ values. The error lines are hidden within individual points – small measurement errors.)

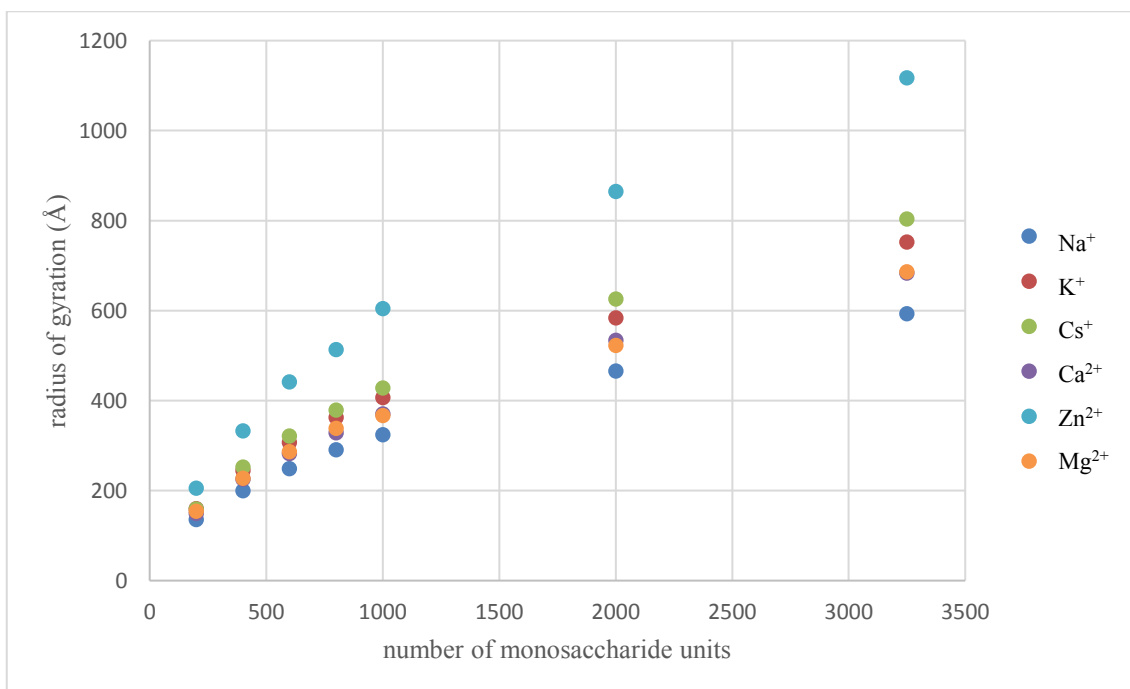


Figure 18 – Dependence of radius of gyration on the number of monosaccharide units ($I = 600$ mmol/l) (The error lines are hidden within individual points – small measurement errors.)

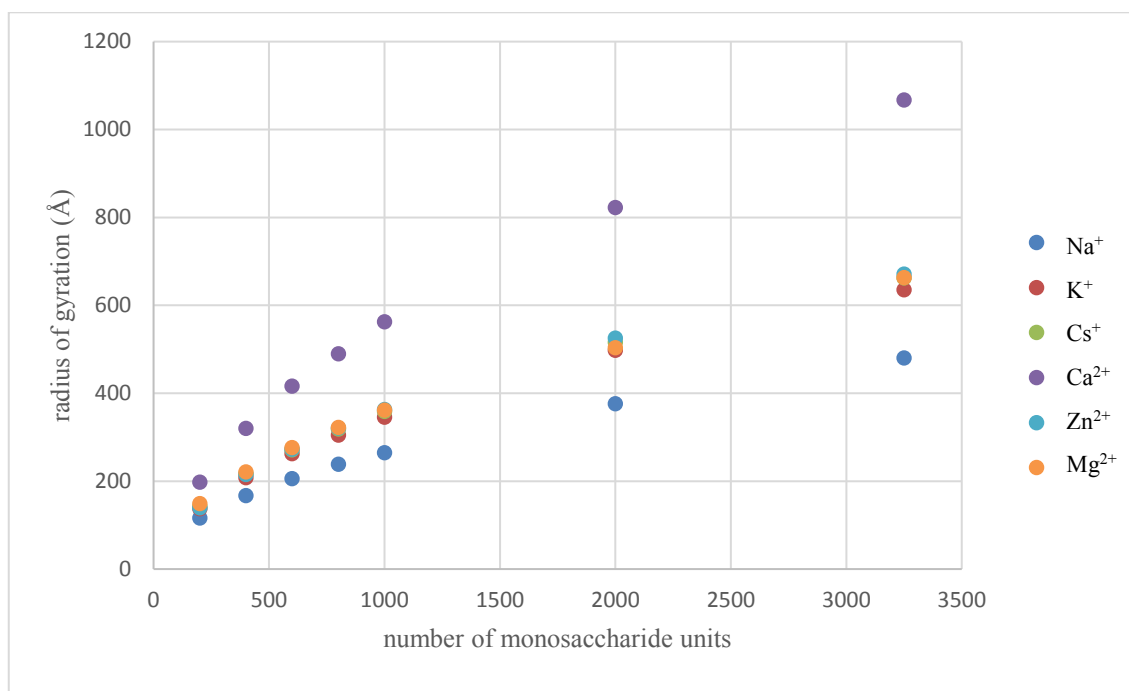


Figure 19 – Dependence of radius of gyration on the number of monosaccharide units ($I = 1000 \text{ mmol/l}$) (The error lines are hidden within individual points – small measurement errors.)

4.2 Hydrodynamic radius

4.2.1 Influence of distributions

The particle size distribution of HA with different molecular mass and various ionic strength is shown on the following figures. On the first three images (Figures 20-22), it can be observed that with increasing molecular weight in the system with sodium ions the particle distribution shows greater symmetry. The higher molecular weight provided us better and more relevant results. The smaller molecular weight increased a measurement error of the particle size. The system with calcium ions evinced a good distribution even for the lowest molecular weight. It could have been caused by faster system stabilization. Systems with divalent ions generally had better particle size distribution –see Figures 23-25.

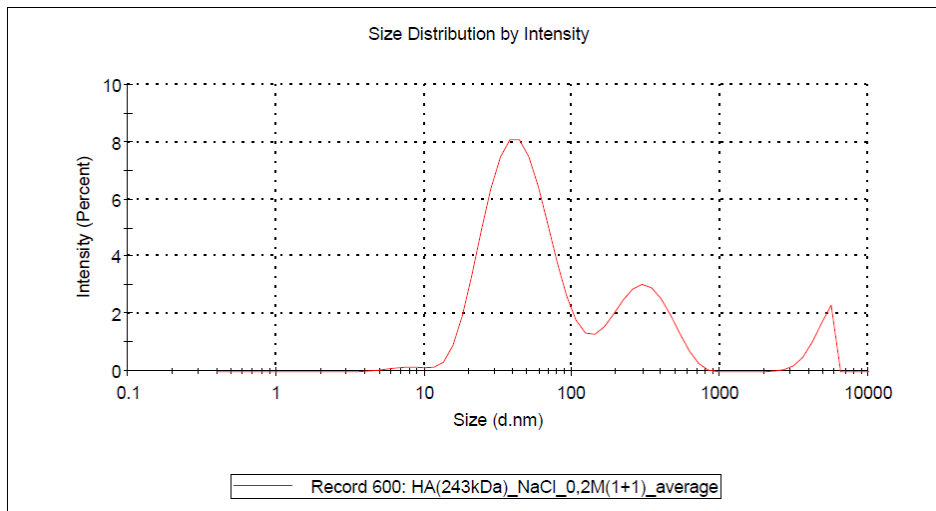


Figure 20 – Particle size distribution for HA ($M_w = 243$ kDa) with sodium ions ($I = 200$ mmol/l)

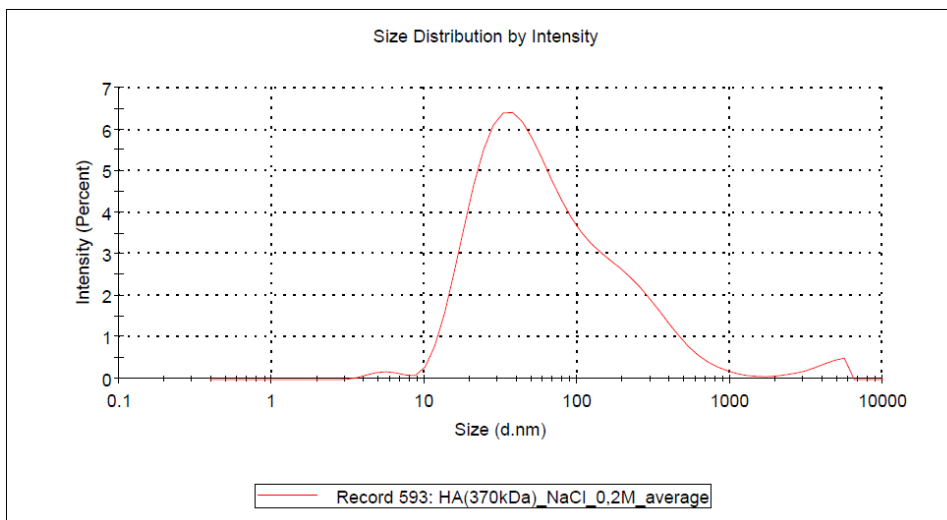


Figure 21 – Particle size distribution for HA ($M_w = 370$ kDa) with sodium ions ($I = 200$ mmol/l)

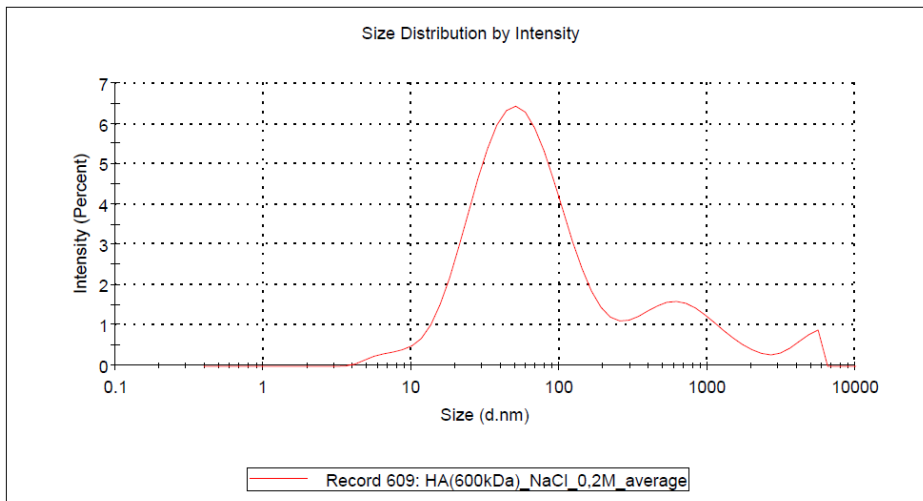


Figure 22 – Particle size distribution for HA ($M_w = 600$ kDa) with sodium ions ($I = 200$ mmol/l)

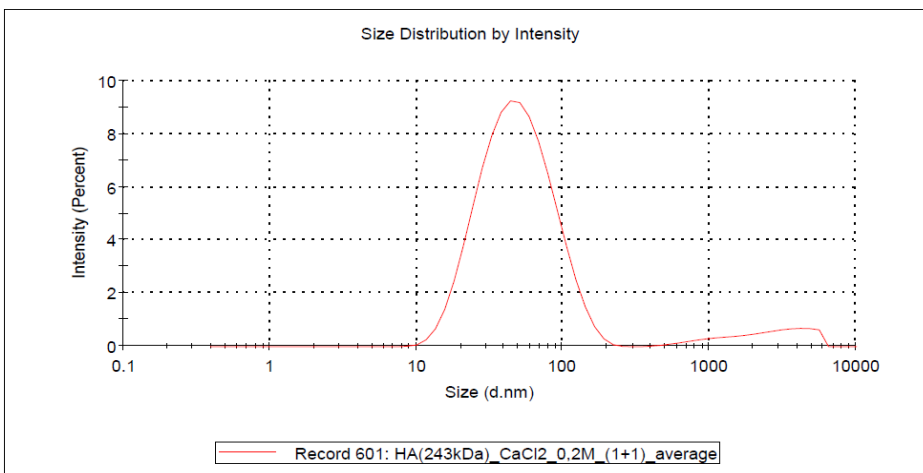


Figure 23 – Particle size distribution for HA ($M_w = 243$ kDa) with calcium ions ($I = 200$ mmol/l)

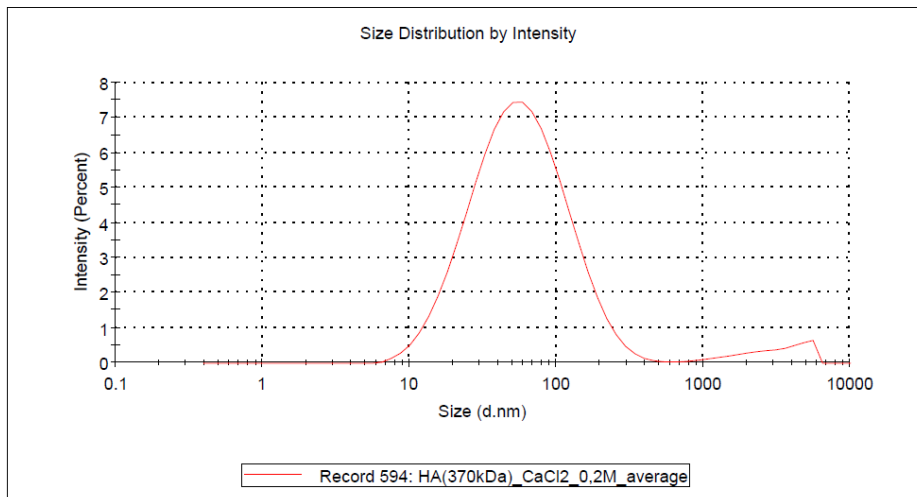


Figure 24 – Particle size distribution for HA ($M_w = 370$ kDa) with calcium ions ($I = 200$ mmol/l)

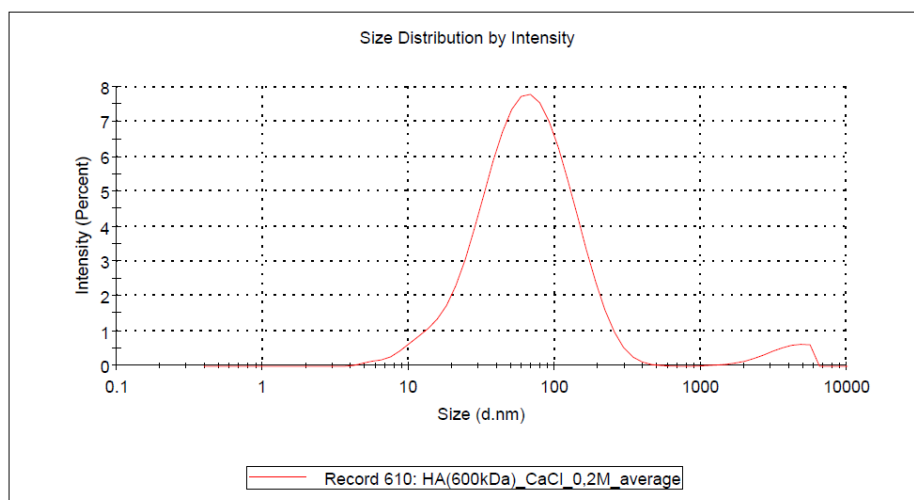


Figure 25 – Particle size distribution for HA ($M_w = 600$ kDa) with calcium ions ($I = 200$ mmol/l)

Particle distribution has also been improved with the ionic strength increase, which could be due to the fact that more ions could cause better stabilization. This fact can be seen on the next two figures (Figure 26 and 27).

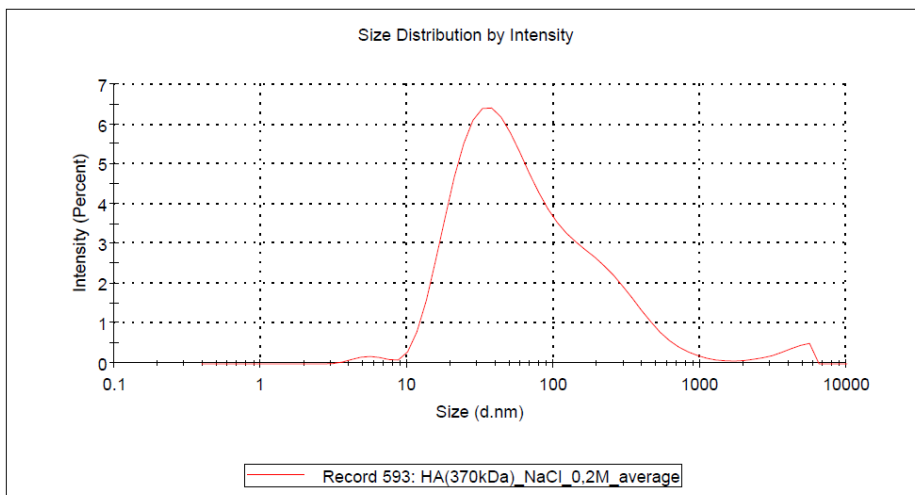


Figure 26 – Particle size distribution for HA ($M_w = 370$ kDa) with sodium ions ($I = 200$ mmol/l)

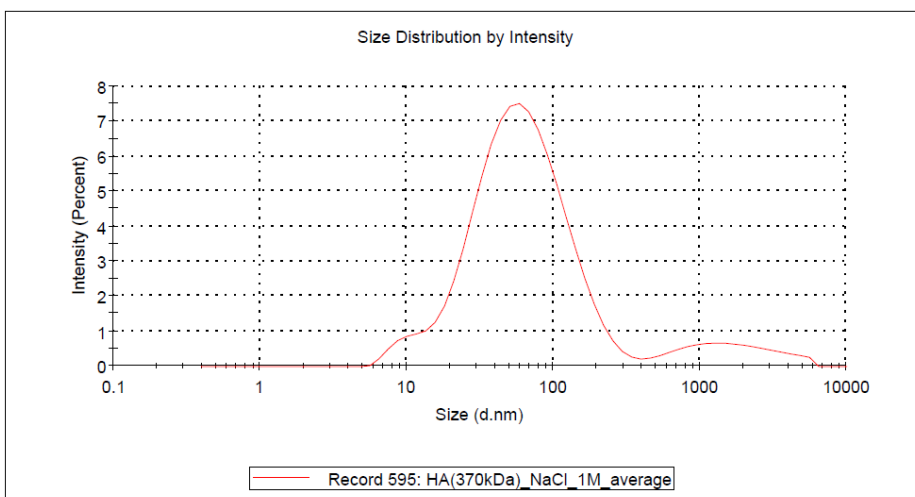


Figure 27 – Particle size distribution for HA ($M_w = 370$ kDa) with sodium ions ($I = 1000$ mmol/l)

4.2.2 Results

HA with the lowest molecular weight (243 kDa) was not evaluated because of high measurement error and different dilution of solutions –see Figure 28. For HA with a medium and larger molecular weight ($M_w = 370$ and 600 kDa), a trend emerged where the greatest hydrodynamic radius was measured at an ionic strength of 600 mmol/l –see Figure 29 and 30. For HA with a molecular weight of 370 kDa (or 600 kDa), the hydrodynamic radius ranged from 390 Å to 530 Å (or from 470 Å to 660 Å). For the medium molecular weight (370 kDa), the hydrodynamic radius for individual measurements did not differ significantly.

Conversely, at the largest molecular weight (600 kDa) there was a meaningful increase in hydrodynamic radius for HA with zinc ions whose value ranged from 580 Å to 660 Å.

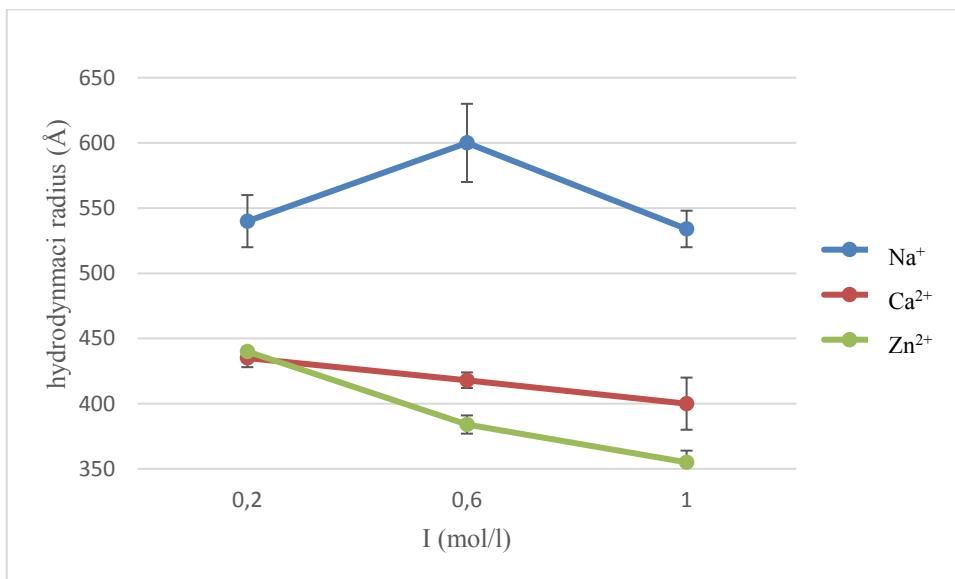


Figure 28 – Dependence of the hydrodynamic radius on ionic strength for individual systems ($M_w = 243$ kDa)

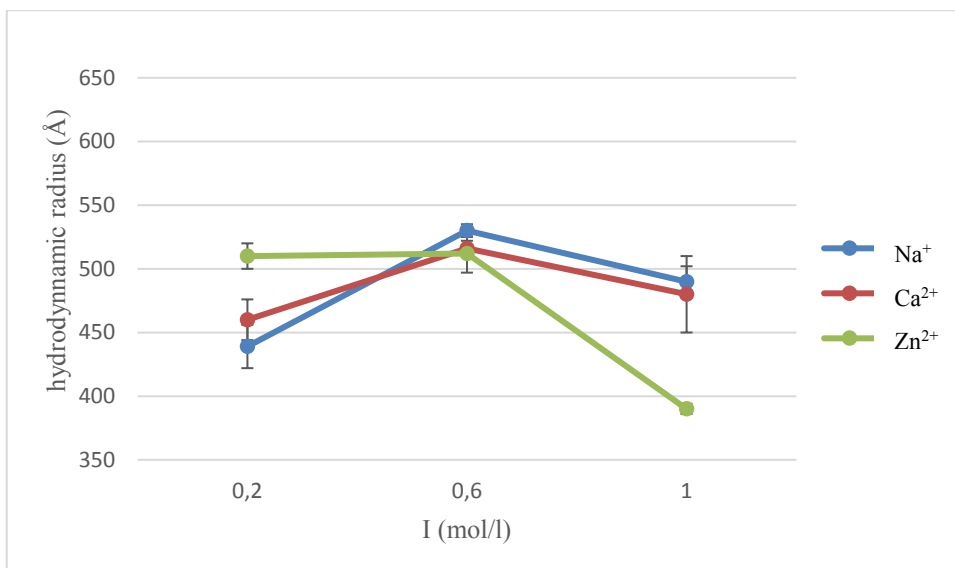


Figure 29 – Dependence of the hydrodynamic radius on ionic strength for individual systems ($M_w = 370$ kDa)

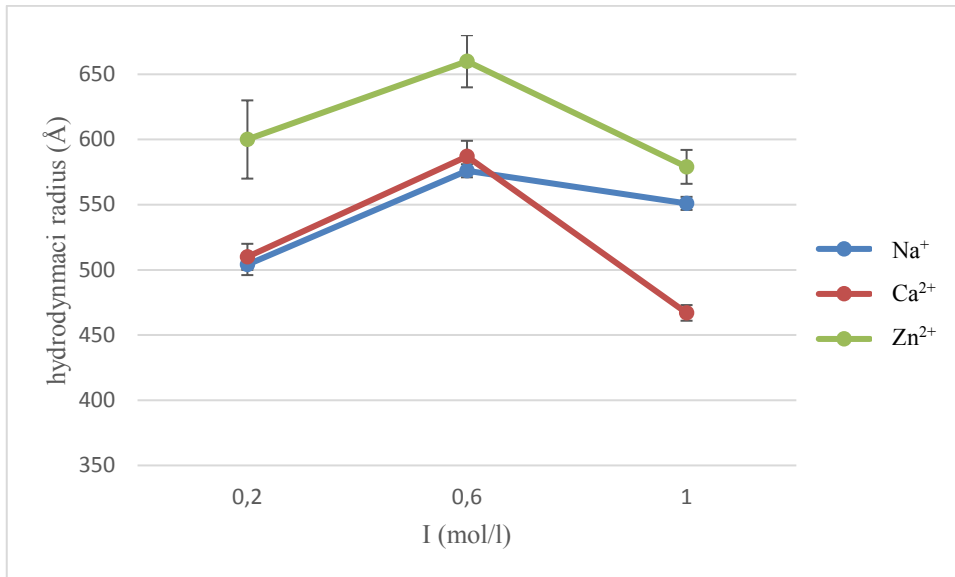


Figure 30 – Dependence of the hydrodynamic radius on ionic strength for individual systems ($M_w = 600$ kDa)

CONCLUSION

The goal of this work was to describe the influence of different ions on the resulting structure of the HA macromolecule, based on molecular dynamics simulations in NAMD software and an experiment using the method of dynamic light scattering. The main intention of this work was to find and provide a possible comparison of these two methods. Two antiparallel chains in water (completely free) with different types of salts (NaCl, KCl, CsCl, CaCl₂, ZnCl₂ and MgCl₂) with various ionic strength (0.2 mol/l, 0.6 mol/l and 1 mol/l) in the vicinity of HA were investigated. Each chain of the system contained 24 pairs of monosaccharide units. The system studied after being surrounded by water was so large that it was for MD at the edge of the tolerability, so that much longer chains can't be explored by molecular dynamics. Subsequently random coils of HA were constructed by application of specific statistical procedure to determine the dihedral angles of glycosidic connections of the pieces. For the experimental part, certain solutions of HA (243 kDa, 370 kDa and 600 kDa) dissolved in saline solution (NaCl, CaCl₂ and ZnCl₂) with different ionic strength (0.2 mol/l, 0.6 mol/l and 1 mol/l) were prepared.

The most interesting discovery was a trend, when both the radius of gyration and the hydrodynamic radius of the coil are the largest for systems with ionic strength of 600 mmol/l. The overall stabilization of the coils and thus the reduction of the radius of gyration and the hydrodynamic radius occurred at the greatest ionic strength (1000 mmol/l). It can be seen in the MD simulations with all salts except calcium. In experiments these trends were observed especially on the systems with zinc ions ($M_w = 370$ kDa) and calcium ions ($M_w = 600$ kDa). The radius of gyration ranged from 300 Å to 865 Å for individual systems and the hydrodynamic radius from 390 Å to 530 Å for the mean molecular weight which corresponds to simulated systems. The different range of these two variables is due to their different nature.

Small disappointment were experimental results for the smallest molecular weight (240 kDa), which showed a big measurement error in hydrodynamic radius and low symmetry of distributions. On the contrary, the system with calcium ions had the smallest measurement error and symmetry distributions for all molecular weights at all ionic strengths. The calcium salt showed excellent and rapid stabilization capabilities. A statistically evident trend in the hydrodynamic radius was mainly observed in the

measurement of HA with the largest molecular weight (600 kDa). It can be clearly stated that at the mean ionic strength (600 mmol/l) the hydrodynamic radius was the largest.

The submitted master's thesis pursued comparison between the radius of gyration from MD simulations and the hydrodynamic radius from experiments (dynamic method). In the future it could be interesting to compare the radius of gyration from MD simulations with the radius of gyration measured by the static light scattering as well.

BIBLIOGRAPHY

- [1] NEČAS, J., L. BARTOŠÍKOVÁ, P. BRAUNER a J. KOLÁŘ. Hyaluronic acid (hyaluronan): a review. *Veterinarni Medicina*. 2008, 53, 397–411
- [2] KOGAN, Grigorij, Ladislav ŠOLTÉS, Robert STERN a Peter GEMEINER. Hyaluronic acid: a natural biopolymer with a broad range of biomedical and industrial applications. *Biotechnol Lett*. 2006, 351, 2-10.
- [3] OUYANG, Liliang, Christopher B. HIGHLEY, Christopher B. RODELL, Wei SUN a Jason A. BURDICK. 3D Printing of Shear-Thinning Hyaluronic Acid Hydrogels with Secondary Cross-Linking. *ACS Biomaterials Science & Engineering* [online]. 2016, 2(10), 1743-1751 [cit. 2018-03-21]. DOI: 10.1021/acsbmaterials.6b00158. ISSN 2373-9878. Available from: <http://pubs.acs.org/doi/10.1021/acsbmaterials.6b00158>
- [4] Průlom v chemii: Čeští vědci zvláknili kyselinu hyaluronovou, použili i "triky". *EuroZprávy.cz* [online]. 2018 [cit. 2018-03-21]. Available from: <http://veda-a-technika.eurozpravy.cz/veda/212951-prulom-v-chemii-cesti-vedci-zvlaknili-kyselinu-hyaluronovou-pouzili-i-triky/>
- [5] BROWN, MB a SA JONES. Hyaluronic acid: a unique topical vehicle for the localized delivery of drugs to the skin. *Journal of the European Academy of Dermatology and Venereology* [online]. 2005, 19(3), 308-318 [cit. 2018-03-21]. DOI: 10.1111/j.1468-3083.2004.01180.x. ISSN 0926-9959. Available from: <http://doi.wiley.com/10.1111/j.1468-3083.2004.01180.x>
- [6] PHILLIPS, James C., James GUMBART, Emad TAJKHORSCHID, Elizabeth VILLA, Christophe CHIPOT, Robert D. SKEEL, Laxmikant KALÉ a Klaus SCHULTEN. Scalable Molecular Dynamics with NAMD. *J Comput Chem*. Beckman Institute, University of Illinois at Urbana-Champaign. 2005, 26(16), 1781–1802.
- [7] INGR, M. *Základy biofyziky* [presentation]. Univerzita Tomáše Bati ve Zlíně. Fakulta technologická, 2015
- [8] SALONEN E. *Introduction to molecular dynamics simulations* [presentation]. Ruhr University, Bochum, October 2006

- [9] Phillips, J.C., Braun, R., Wang, W., Gumbart, J., Tajkhorshid, E., Villa, E., Chipot, Ch., Skeel, R.D., Kale, L., Schulten, K. Scalable molecular dynamics with NAMD. *J. Comput. Chem.* 2005, 26, 1781-1802.
- [10] Brooks, B.R., Bruccoleri, R.E., Olafson, B. D., States, D. J., Swaminathan, S., Karplus, M. CHARMM: A Program for Macromolecular Energy, Minimization, and Dynamics Calculations, *J. Comp. Chem.* 1983, 4, 187-217.
- [11] NAMD User's Guide Version 2.10. [online]. Available from <http://www.ks.uiuc.edu/Research/namd/> [cit. 2018-03-21].
- [12] LOBANOV, M. Yu., N. S. BOGATYREVA a O. V. GALZITSKAYA. Radius of gyration as an indicator of protein structure compactness. *Molecular Biology* [online]. 2008, 42(4), 623-628 [cit. 2018-03-21]. DOI: 10.1134/S0026893308040195. ISSN 0026-8933. Available from: <http://link.springer.com/10.1134/S0026893308040195>
- [13] MEHTA, Pooja. Dynamic light Scattering [online]. 2014 [cit. 2018-03-21]. Available from: <https://www.slideshare.net/poojabhartii3/dynamic-light-scattering>
- [14] SORCI, Gina A. a Wayne F. REED. Effect of Valence and Chemical Species of Added Electrolyte on Polyelectrolyte Conformations and Interactions. *Macromolecules*. 2003, 2004(37), 554-565.
- [15] FOUISSAC, E., M. MILAS, M. RINAUDO a R. BORSALI. Influence of the Ionic Strength on the Dimensions of Sodium Hyaluronate. *Macromolecules*. 1991, 1992(25), 5613-5617.
- [16] HAYASHI, Kanako, Fumio NAKAJIMA, Takashi NORISUYE and Akio TERAMOTO. Chain-Stiffness and Excluded-Volume Effects in Solutions of Sodium Hyaluronate at High Ionic Strength. *Macromolecules*. 1994, 1995(28), 3824-3830.
- [17] MENDICHI, Raniero, Ladislav ŠOLTÉS a Alberto Giacometti SCHIERONI. Evaluation of Radius of Gyration and Intrinsic Viscosity Molar Mass Dependence and Stiffness of Hyaluronan. *Macromolecules*. 2002, 2003(4), 805-1810.
- [18] BUHLER, Eric, Francois Boue. Chain Persistence Length and Structure in Hyaluronan Solutions: Ionic Strength Dependence for a Model Semirigid Polyelectrolyte. *Macromolecules*. 2004, 37, 1600-1610.

- [19] ZAGROVIC, Bojan, Guha JAYACHANDRAN, Ian S. MILLETT, Sebastian DONIACH a Vijay S. PANDE. How Large is an α -Helix? Studies of the Radii of Gyration of Helical Peptides by Small-angle X-ray Scattering and Molecular Dynamics. *Journal of Molecular Biology* [online]. 2005, 353(2), 232-241 [cit. 2018-03-21]. DOI: 10.1016/j.jmb.2005.08.053. ISSN 00222836. Available from: <http://linkinghub.elsevier.com/retrieve/pii/S0022283605010077>
- [20] INGR, Marek, Eva KUTÁLKOVÁ and Josef HRNČIŘÍK. Hyaluronan random coils in electrolyte solutions—a molecular dynamics study. *Carbohydrate polymers*. 2017, 170, 289-295
- [21] IVANOV, D., A. NEAMTU. Molecular dynamics evaluation of Hyaluronan interactions with dimethylsilanediol in aqueous solution. *Rev. Roum. Chim.* 2013, 229-238
- [22] ALMOND, A. P.L. DeANGELIS and Ch. D. BLUNDELL. Hyaluronan: The Local Solution Conformation Determined by NMR and Computer Modeling is Close to a Contracted Left-handed 4-Fold Helix. *J. Mol. Biol.* 2006, 358-359
- [23] PECORA, R. Dynamic light scattering measurement of nanometer particles in liquids. *Journal of Nanoparticle Research*. Kluwer Academic Publishers, 2000, 2, 123–131
- [24] HOO, Christopher M., Natasha STAROSTIN, Paul WEST a Martha L. MECARTNEY. A comparison of atomic force microscopy (AFM) and dynamic light scattering (DLS) methods to characterize nanoparticle size distributions. *Journal of Nanoparticle Research* [online]. 2008, 10(S1), 89-96 [cit. 2018-03-21]. DOI: 10.1007/s11051-008-9435-7. ISSN 1388-0764. Available from: <http://link.springer.com/10.1007/s11051-008-9435-7>.
- [25] MALCOLM P. STEVENS. *Polymer Chemistry: An Introduction*. 2nd Ed. New York: Oxford University Press, 1990. ISBN 0195066472.
- [26] GRUNDĚLOVÁ, Lenka, Aleš MRÁČEK, Věra KAŠPÁRKOVÁ, Antonín MINAŘÍK a Petr SMOLKA. The influence of quaternary salt on hyaluronan conformation and particle size in solution. *Carbohydrate Polymers* [online]. 2013, 98(1), 1039-1044 [cit. 2018-03-21]. DOI: 10.1016/j.carbpol.2013.06.057. ISSN 01448617. Available from: <http://linkinghub.elsevier.com/retrieve/pii/S014486171300653X>

- [27] GRIBBON, Phillip, Boon Chin HENG a Timothy E. HARDINGHAM. The analysis of intermolecular interactions in concentrated hyaluronan solutions suggest no evidence for chain–chain association. *Biochem. J.* 2000, 350, 329-335.
- [28] VILLETTI, Marcos A., Redouane BORSALI, Janaina S. CRESPO, Valdir SOLDI a Kazuhiro FUKADA. Static and Dynamic Light Scattering of Polyelectrolyte/Surfactant Solutions: the Na-Hyaluronate/(C10TAB) System. *Macromolecular Chemistry and Physics* [online]. 2004, 205(7), 907-917 [cit. 2018-03-21]. DOI: 10.1002/macp.200300192. ISSN 1022-1352. Available from: <http://doi.wiley.com/10.1002/macp.200300192>
- [29] VMD User's Guide Version 1.9.3 [online]. Available from <http://www.ks.uiuc.edu/Research/vmd/current/ug/> [cit. 2018-03-30].
- [30] FURLAN, Sara, Giovanni LA PENNA, Angelo PERICO and Attilio CESÀRO. Hyaluronan chain conformation and dynamics. *Carbohydrate Research* [online]. 2005, 340(5), 959-970 [cit. 2018-05-05]. DOI: 10.1016/j.carres.2005.01.030. ISSN 00086215. Available from: <http://linkinghub.elsevier.com/retrieve/pii/S0008621505000649>
- [31] Zetasizer Nano Series User Manual 1.1 [online]. Available from http://www.biophysics.bioc.cam.ac.uk/files/Zetasizer_Nano_user_manual_Man0317-1.1.pdf [cit. 2018-03-31].

LIST OF ABBREVIATIONS

HA	Hyaluronan
MD	Molecular dynamics
c	Concentration
M _w	Molecular weight
CH	Carbohydrates
NAMD	Nanoscale Molecular Dynamics
CHARMM	Chemistry at Harvard Macromolecular Mechanics
R _g	Radius of gyration
NaHy	Sodium Hyaluronate
CaHy	Calcium Hyaluronate
SAXS	Small-angle X-ray scattering
DLS	Dynamic light scattering
PCS	Photon Correlation Spectroscopy
PSF	Protein Structure File
VMD	Virtual Molecular Dynamics
vdW	van der Waals

LIST OF FIGURES

Figure 1 – The primary, secondary and tertiary structures of HA in solutions.	13
Figure 2 – Basic principle of calculation	15
Figure 3 – Graph of VDW potential with and without cutoff function	16
Figure 4 – Radius of gyration (s)	18
Figure 5 – Dependence of radius of gyration on ionic strength.....	19
Figure 6 – Radius of gyration results for different molecular weight M_w and concentration c	20
Figure 7 – Radius of gyration of NaHy for different M_w	20
Figure 8 – Radius of gyration as a function of the number of monosaccharide units N for all the simulated systems	22
Figure 9 – Schematic diagram of a PCS apparatus.....	24
Figure 10 – Hydrodynamic radius (the size of a hypothetical hard sphere that diffuses in the same fashion as the particle being measured)	25
Figure 11 – Phase diagram of Na-Hy polyelectrolyte in C10TAB surfactant and NaCl salt. (I) homogeneous phase; (II) phase separation and (III) homogeneous phase after addition of salt or surfactant.	26
Figure 12 – Double-chain of HA	28
Figure 13 – Dependence of the mean number of Ca^{2+} N ions in the vicinity of HA on time.....	30
Figure 14 – Dependence of HA-HA electrostatic interactions on the ionic strength for individual systems	34
Figure 15 – Dependence of the radius of gyration on ionic strength for individual systems	35
Figure 16 – Dependence of the number of ions in the vicinity of HA on ionic strength for individual systems	36
Figure 17 – Dependence of radius of gyration on the number of monosaccharide units ($I = 200$ mmol/l)	37
Figure 18 – Dependence of radius of gyration on the number of monosaccharide units ($I = 600$ mmol/l)	37
Figure 19 – Dependence of radius of gyration on the number of monosaccharide units ($I = 1000$ mmol/l)	38

Figure 20 – Particle size distribution for HA ($M_w = 243$ kDa) with sodium ions ($I = 200$ mmol/l)	39
Figure 21 – Particle size distribution for HA ($M_w = 370$ kDa) with sodium ions ($I = 200$ mmol/l)	39
Figure 22 – Particle size distribution for HA ($M_w = 600$ kDa) with sodium ions ($I = 200$ mmol/l)	40
Figure 23 – Particle size distribution for HA ($M_w = 243$ kDa) with calcium ions ($I = 200$ mmol/l)	40
Figure 24 – Particle size distribution for HA ($M_w = 370$ kDa) with calcium ions ($I = 200$ mmol/l)	41
Figure 25 – Particle size distribution for HA ($M_w = 600$ kDa) with calcium ions ($I = 200$ mmol/l)	41
Figure 26 – Particle size distribution for HA ($M_w = 370$ kDa) with sodium ions ($I = 200$ mmol/l)	42
Figure 27 – Particle size distribution for HA ($M_w = 370$ kDa) with sodium ions ($I = 1000$ mmol/l)	42
Figure 28 – Dependence of the hydrodynamic radius on ionic strength for individual systems ($M_w = 243$ kDa)	43
Figure 29 – Dependence of the hydrodynamic radius on ionic strength for individual systems ($M_w = 370$ kDa)	43
Figure 30 – Dependence of the hydrodynamic radius on ionic strength for individual systems ($M_w = 600$ kDa)	44

LIST OF TABLES

Table 1 – Results of radius of gyration for different M_w	21
Table 2 – Results of radius of gyration	21
Table 3 – Minimal HA-HA interaction energy values (kcal/mol) for individual systems from all simulation runs	33

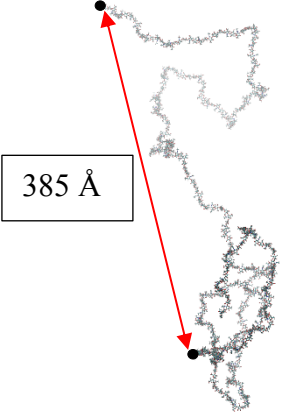


APPENDICES

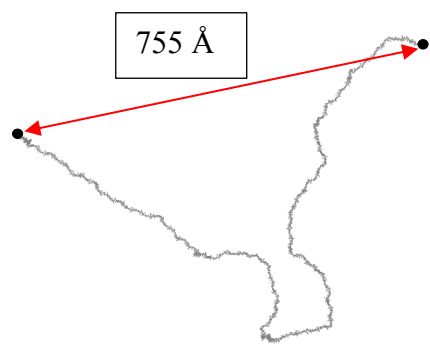

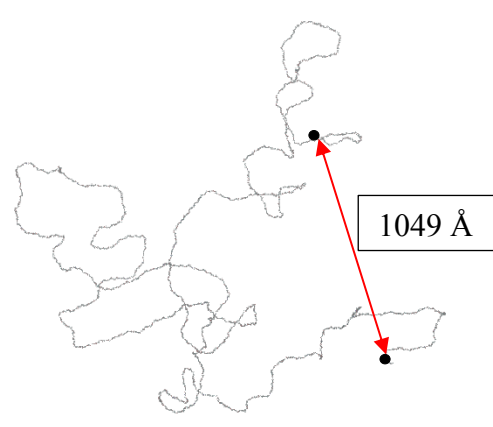
APPENDIX P I: CONFIGURATION FILE .NAMD	56
APPENDIX P II: FIGURES OF INDIVIDUAL COILS.....	57

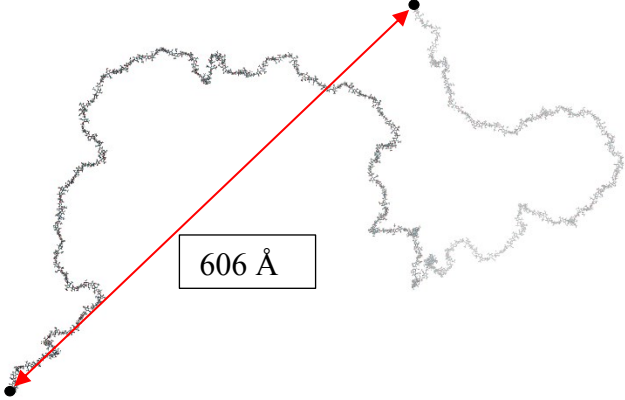

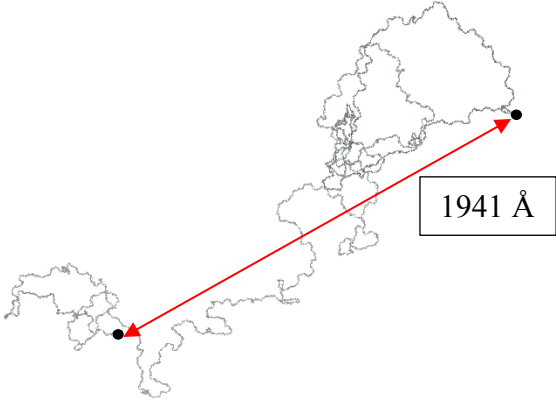
APPENDIX P I: CONFIGURATION FILE .NAMD

```
structure /storage/brno6/home/v_bus/K/2wild_K_1M.psf
coordinates /storage/brno6/home/v_bus/K/2wild_K_1M.pdb
set temperature 310
set outputname /storage/brno6/home/v_bus/K/2wild_K_1M
firsttimestep 0
# Input
paraTypeCharmm on
parameters /storage/brno6/home/v_bus/par_top.inp
temperature $temperature
# Force-Field Parameters
exclude scaled1-4
1-4scaling 1.0
cutoff 10.0
switching on
switchdist 8.0
pairlistdist 12.0
# Integrator Parameters
timestep 1.0 ;# 1fs/step
rigidBonds water
molly on
nonbondedFreq 2
fullElectFrequency 6
stepspercycle 30
# Constant Temperature Control
langevin on ;# do langevin dynamics
langevinDamping 1 ;# damping coefficient (gamma) of 1/ps
langevinTemp $temperature
langevinHydrogen off ;# don't couple langevin bath to hydro-gens
# Periodic Boundary Conditions
cellBasisVector1 161.8 0.0 0.0
cellBasisVector2 0.0 110.9 0.0
cellBasisVector3 0.0 0.0 187.2
cellOrigin 75.4 39.7 -50.5
wrapWater on
wrapAll on
# PME (for full-system periodic electrostatics)
PME yes
PMEGridSpacing 1.0
# Constant Pressure Control (variable volume)
useGroupPressure yes ;# needed for rigidBonds
useFlexibleCell no
useConstantArea no
```


APPENDIX P II: FIGURES OF INDIVIDUAL COILS

Number of units	System with Na ⁺ (I = 1000 mmol/l)
400	 <p>A diagram showing a vertical, elongated coil structure. Two black dots are placed at the top and bottom of the structure. A red double-headed arrow connects these two dots, with a label box containing the text "385 Å".</p>
2000	 <p>A diagram showing a more complex, branched coil structure. Two black dots are placed at the top and bottom of the main vertical stem. A red double-headed arrow connects these two dots, with a label box containing the text "573 Å".</p>
3250	 <p>A diagram showing a highly branched and elongated coil structure. Two black dots are placed at the top and bottom of the structure. A red double-headed arrow connects these two dots, with a label box containing the text "1751 Å".</p>

Number of units	System with Ca^{2+} ($I = 1000 \text{ mmol/l}$)
400	 <p>A diagram showing a single, irregularly shaped unit. A red double-headed arrow spans the width of the unit, with a box above it containing the text "755 Å".</p>
2000	 <p>A diagram showing a larger, more complex irregularly shaped unit. A red double-headed arrow spans a portion of its width, with a box above it containing the text "801 Å".</p>
3250	 <p>A diagram showing a highly complex, multi-lobed irregularly shaped unit. A red double-headed arrow spans across two lobes, with a box above it containing the text "1049 Å".</p>

Number of units	System with Zn ²⁺ (I = 1000 mmol/l)
400	 <p>A diagram showing a complex, irregular shape representing a system with 400 units. A red double-headed arrow spans a portion of the shape, with a label '606 Å' in a box next to it.</p>
2000	 <p>A diagram showing a more complex, irregular shape representing a system with 2000 units. A red double-headed arrow spans a portion of the shape, with a label '1184 Å' in a box next to it.</p>
3250	 <p>A diagram showing a highly complex, irregular shape representing a system with 3250 units. A red double-headed arrow spans a portion of the shape, with a label '1941 Å' in a box next to it.</p>